The fingerprints of flexure in slab seismicity

D. Sandiford[1,2,3], L.M Moresi[2,4,], M. Sandiford[2], R. Farrington[2], T. Yang[5]

[1]Institute of Marine and Antarctic Studies, University of Tasmania

[2]School of Earth Sciences, University of Melbourne

[3]Helmholtz Centre Potsdam - German Research Centre for Geosciences (GFZ)

[4]Australian National University

[5]Southern University of Science and Technology

Key Points:

- Intermediate depth seismicity is controlled by bending in a wide range of settings
- Geometric differences lead to contrasting seismic expression between east and west Pacific slabs
- Double seismic zones associated with bending are often masked by the strong temperature controls on seismicity

---

Corresponding author: Dan Sandiford, `dan.sandiford@utas.edu.au`

Abstract

East Pacific (ePac) slabs are characterised by downdip tension (DT) at intermediate depths, whereas most west Pacific (wPac) slabs are dominated by downdip compression (DC, e.g. Tonga) or have mixed mechanisms indicative of unbending (e.g. Kuriles). In this study we argue that despite these contrasts, flexural modes associated with slab bending/unbending govern the seismic expression of slabs in both settings, thus challenging the prevailing paradigm that slab strain rates are dominated by uniform modes (stretching or shortening). Firstly, we demonstrate that earthquake clusters consistent with slab unbending are present in ePac slabs, in addition to previously recognized wPac locations. A key difference is that unbending takes place at much shallower depths in ePac slabs, often ceasing at around 60 km, whereas unbending in wPac slabs can extend beyond 200 km. We then show how systematic geometric differences between ePac and wPac slabs leads to additional zones of bending at intermediate depths in ePac slabs. The majority of ePac DT seismicity is clustered in curvature-increasing (+ve bending rate) zones associated with full or partial slab flattening. We argue that because seismicity is restricted to the colder parts of slabs at temperatures below about 600°C, typically only the extensional upper part of these +ve bending rate zones are seismically active. Below the neutral plane, the corresponding shortening is mostly accommodated aseismically thereby masking the development of diagnostic polarized double seismic zones expected for flexural modes. We illustrate our hypothesis with results from a numerical subduction model in which geometry-controlled flexural modes dominate the slab deformation rate. While our framework is consistent with the notion that geometric controlled deformation dominates slab strain rates, we argue that the expression of slab buoyancy (e.g. slab pull) is discernible in terms of a systematic modifying effect on the seismic expression of flexure.

1 Introduction

Plate motions are driven primarily by density heterogeneities in the mantle. It is generally accepted that the most important density heterogeneities are associated with the oceanic plates where they sink into the mantle at subduction zones (Conrad & Lithgow-Bertelloni, 2002; Elsasser, 1969; McKenzie, 1969). Inclined zones of earthquakes beneath arcs delineate the geometry of these subducting slabs and provide a unique insight into slab dynamics. To the extent that rupture mechanisms of intermediate depth earthquakes

are thought to reflect, at least to some degree, the force balance in subducting slabs, they have been used to provide key insights into the basic mechanisms of plate tectonics. The force system in slabs include buoyancy forces due to thermal and metamorphic density contrasts, flexural stress associated with slab bending and unbending, and resistance arising from slip along the subduction interface and deeper mantle penetration (e.g. Fujita & Kanamori, 1981a; House & Jacob, 1982; Isacks & Molnar, 1971; Sleep, 1979).

Intermediate-depth earthquakes have traditionally been defined as those in the $\sim$ 70-300 km depth range, where the subducting slab is detached from the over-riding plate (Gutenberg & Richter, 1954). The studies of (Isacks & Molnar, 1969, 1971) provided a number of enduring insights related to intermediate depth slab seismicity. They showed that the least/most extensive eigenvectors of earthquake moment tensors tend to be aligned in the slab downdip direction, consistent with the slab acting as a stress guide in a weaker mantle (Elsasser, 1969). They also identified that the co-seismic deformation patterns at intermediate depths correlate with broader seismic distribution in the slab. Slabs segments with no deep earthquakes, or significant gaps between intermediate and deep earthquakes, usually exhibit downdip tension/stretching (DT). (The notion of tension here refers to an effective rather than an absolute state of tension). In contrast, slabs with deep and continuous seismicity tend to be dominated by downdip compression/shortening (DC). Based on these spatial relationships, Isacks and Molnar (1971) helped to establish the prevailing paradigm that slab earthquake orientations mainly reflect uniaxial, or uniform, stress/strain modes. To quote a recent study "slabs seem to be stretching as gravity acting on excess mass in the slabs pulls them down, like dangling springs hanging from and attached to lithosphere above" (Molnar & Bendick, 2019).

The correlations identified by Isacks and Molnar (1971) relate to the seismicity patterns in individual slab segments, yet they also expose contrasts in the seismic expression between slabs along the eastern margin of the Pacific Ocean (ePac) and those along the western margin (wPac). In ePac slabs, intermediate depth focal mechanisms are strongly dominated by DT earthquakes. The Nazca slab in Chile is seen as archetypal ePac DT setting, which is often attributed to stretching due to slab pull (Bailey, Becker, & Ben-Zion, 2009; Bloch, Schurr, Kummerow, Salazar, & Shapiro, 2018; Isacks & Molnar, 1971; Rietbrock & Waldhauser, 2004). This contrasts most strikingly with wPac Pacific Plate subduction beneath Tonga, where intermediate depth focal mechanisms are dominated by DC events. DC regimes have been attributed to the propagation of compressional stress

along the slab from interactions between the deep parts of the slab and the transition zone (Billen, Gurnis, & Simons, 2003; Fujita & Kanamori, 1981b; Gurnis, Ritsema, Heijst, & Zhong, 2000).

The role of flexural deformation has mainly been discussed in relation to Pacific Plate subduction, e.g. northern Japan, Kuriles, Tonga, northern Marianas and eastern Aleutians. In these regions intermediate depth focal mechanisms exhibit a systematic polarity switch, suggesting that the upper part of the slab mantle is in downdip compression while the lower part is in down dip tension (Engdahl & Scholz, 1977; Hasegawa, Umino, & Takagi, 1978; Kawakatsu, 1986a, 1986b; Kita, Okada, Hasegawa, Nakajima, & Matsuzawa, 2010; Samowitz & Forsyth, 1981; Sleep, 1979; Tsukahara, 1980; Wang, 2002). These Double Seismic Zones (DSZ) are consistent with unbending in the presence of dehydration embrittlement. Other studies have noted regional correlations between geometry (i.e. 'warping' or 'flexure') and seismicity, particularly in shallow slab settings (Craig & Copley, 2018; McCrory, Blair, Waldhauser, & Oppenheimer, 2012).

However, because some DSZs continue beyond the expected depths of unbending, and others have an opposite polarity to that expected from slab unbending (Comte et al., 1999), additional sources of stress have been argued to play a significant role in localising DSZ seismicity (Brudzinski, Thurber, Hacker, & Engdahl, 2007; Fujita & Kanamori, 1981b). Other studies have focused on DSZs as a metamorphic/dehydration phenomena, without explicit consideration of the contribution the stress field in which they nucleate (Peacock, 2001). Indeed, while metamorphic and fluid processes have long been seen as necessary ingredient for intermediate depth nucleation (e.g. Isacks & Molnar, 1971), this metamorphic framework has come to dominate discussions of slab seismicity in recent decades (Chen, Manea, Niu, Wei, & Kiser, 2019; Faccenda, 2014; Green & Houston, 1995; Hacker, Peacock, Abers, & Holloway, 2003; Kirby, Engdahl, & Denlinger, 2013; Peacock, 2001; Seno & Yamanaka, 2013; Tsujimori, Sisson, Liou, Harlow, & Sorensen, 2006).

Even allowing for the strong weakening role played by dehydration, the concept that some slabs undergo appreciable rates of stretching (10^{-15} s^{-1}, (e.g. Kawakatsu, 1986a)) implies high deviatoric stresses. This is because uniform stretching involves not only the brittle deformation of weakened (e.g. fluid-overpressured) crust and mantle, but also deformation of the deeper, ductile slab core (e.g. F. A. Capitanio, Morra, & Goes, 2009).

Conrad and Lithgow-Bertelloni (2004) argued that effective tensional stress magnitudes may be as much as 500 MPa, in order to produce bulk stretching rates in the order of 10^{-15} s^{-1}, assuming effective slab viscosity several hundred times higher than a typical upper mantle value. While uncertainties in slab rheology mean such high stress estimates are speculative, these magnitudes lie in the range of plausible estimates, given that the thermal and compositional buoyancy forces in subducting slabs are of order 10^{13} N.m^{-1}.

In this study we argue that flexural modes accompanying slab bending and unbending provide an important control on the seismic moment release in many Pacific margin slab segments, but in ways that are subtly obscured by thermal controls. We show, firstly, that earthquakes due to slab unbending are much more widespread than previously recognised, occurring in both ePac and wPac slabs. An important difference between ePac and wPac slabs is that unbending takes place at much shallower depth in the former. Hence, most ePac unbending earthquakes have strong spatial overlap with the megathrust zone, and so have been largely overlooked in previous analyses. In section 3 we describe a procedure to filter megathrust earthquakes from global catalogs, that helps reveal this characteristic ePac signature of shallow unbending.

We then show how systematic geometric complexities lead to additional zones of bending in ePac slabs, that are absent in wPac slabs. The majority of ePac DT seismicity is conspicuously clustered in curvature-increasing zones associated with full or partial slab flattening. In such zones, we speculate that seismicity is mainly restricted to the cold, upper half of the slabs, where they evidence down-dip stretching and that the associated shortening in the lower half of the slab is largely accommodated aseismically. Crucially, while the larger earthquakes, as found in the global CMT catalog, have uniform DT seismicity in Chile, microseismic studies have revealed an oppositely-polarised DSZs (Comte & Suarez, 1994), consistent with the model presented here. The framework implies that strain rates associated geometric bending/unbending rates are larger than those associated uniform stretching modes due to, for example, slab pull. This is consistent with the notion that slab buoyancy is largely supported by drag in the upper mantle.

141   **Notes on terminology**

142   In this section we clarify the terminology we use in discussing seismicity and slab

143   dynamics. Intermediate-depth earthquakes are traditionally defined as those lying in the

144   70-300 km depth range $\sim$ 70-300 km depth range. As we will show, the somewhat ar-

145   bitrary restriction to events deeper than about 70 kms has imposed some important lim-

146   itations. We will use term 'slab' or 'intraslab' earthquakes to refer to all earthquakes in

147   the subducting lithosphere: that is, from the onset of bending of the plate (tradition-

148   ally called outer-rise earthquakes) to the deepest limit of seismicity ($\sim$ 700 km). How-

149   ever, our analysis focuses only on earthquakes shallow than 300 km. The reasons for this

150   restriction are: 1) constraints on slab geometry and accuracy of earthquake hypocenters

151   are likely to decrease with greater depth; 2) the global distribution of slab earthquakes

152   shows a local minimum at around 300 km depth (e.g. Vassiliou, Hager, & Raefsky, 1984).

153   On the other hand, our analysis assumes no intrinsic distinction between earthquakes

154   above and below 70 km. We will still occasionally refer to intermediate depths, as this

155   remains a valid (and familiar) specification of a particular depth range.

156   The term outer-rise earthquakes is potentially a misnomer, because earthquakes

157   that result from curvature increase of the incoming plate are limited not only to the outer

158   rise, but in some slabs extends landward of the trench, beneath the shallow part of the

159   fore-arc. Hence we will refer to the region where the incoming plate experiences increas-

160   ing curvature as 'outer bending zone' (or OBZ). Downdip of the OBZ, after passing through

161   peak curvature, slabs invariably straighten in a zone of unbending which we term the

162   primary unbending zone (or PUZ).

163   In discussing contributions to the slab deformation rate, we emphasise the distinc-

164   tion between uniform modes and flexural/bending modes. We use the terms flexure and

165   bending somewhat interchangeably, in keeping with historical developments in the lit-

166   erature. Flexural strain (rates) is associated with changes in curvature. Curvature is con-

167   sidered positive when the plate/slab is concave down, which means that the slab hinge

168   in typical subduction zones has positive curvature. For reasons that will be discussed

169   in more detail, our analysis makes the assumption that strain (rates) associated with bend-

170   ing is two-dimensional (related to changes in curvature in the downdip direction). Strain

171   rates due to flexural deformation are characterised by an anti-symmetry across the neu-

172   tral plane. The polarity depends on the sign of the bending rate: positive bending rates,

where where curvature is increasing, are associated with downdip extension above the neutral plane and downdip compression below. Arguments that slab seismicity is controlled by bending/unbending, are based on the identification of an analogous polarity switch in earthquake moment tensors. In referring to 'uniform' modes of deformation, we mean either bulk slab stretching or shortening in the downdip direction. The prevailing paradigm for slab seismicity emphasises uniform deformation modes, particularly in connection with ePac DT zones (e.g. Isacks & Molnar, 1971).

It is important to note that our use of the term flexure is essentially divorced from the context of elastic sheet mechanics, where the term flexure is also very common. If slabs behaved as competent elastic sheets, we would expect that stress would vary systematically with the total curvature, and in the process of unbending the plate would simply return to an undisturbed elastic state. An important conclusion of our study (reinforcing a range of previous arguments) is that the instantaneous elastic strain contribution in slabs is a relatively minor component of the total flexural deformation.

2 Data

2.1 Slab geometry and region selection

In this study we consider ePac slab segments in Chile, Peru and Central America, and wPac slab segments in Tonga, Japan (northern Honshu) and the Kuriles. The seismic expression of these regions is described in Section 4. An important component of our analysis involves correlations between measures of downdip slab geometry (e.g. curvature gradient) and the seismic expression. A convenient way of assessing these relationships is by using regional sections across the subduction system, in which patterns of aggregated seismicity (trench parallel) can be compared to the characteristic slab geometry.

In choosing regions suitable for analysis, a balance is sought between slab segments that encompass sufficient well constrained slab earthquakes, while also having a relatively strong morphological similarity along strike. The complicating issue, which we discuss later in more detail, is that the greater the along-strike distance, the more variability in morphology, the very effects of which we are seeking to isolate.

Using either the Slab1 and Slab2 models (Hayes et al., 2018; Hayes, Wald, & Johnson, 2012) we construct regionally-averaged slab surface profiles. We begin by interpo-

lating the chosen slab model along a series of trench perpendicular lines spaced at approximately 10 km intervals along the trench. The azimuth of these lines is shown in the region maps (e.g Fig. 3). Because the slab models do not always extend to the trench, we build a spline representation between the regionally-averaged slab model profile and bathymetry data from ETOPO1 (Amante & Eakins, 2009), thus providing a continuous representation of the slab model that extends well into the surface oceanic plate. We then average these individual profiles to generate a single representative slab surface geometry that provides a consistent fit to the earthquake hypocenters at intermediate depths.

Like earthquake hypocenters, the 3D morphology of slabs in the upper mantle is subject to uncertainty, particularly in regions where seismicity is sparse and/or slab morphology is inherently complex. The recent Slab2 surface model (Hayes et al., 2018) uses multiple input data types to augment earthquake-derived slab geometry models. The use of multiple input data sources in the Slab2 model is likely to improve the overall accuracy of the subduction geometry, however in doing so it appears to sacrifice consistency with earthquake hypocenter data in some locations. This problem is particularly evident in Tonga, where the Slab2 model clearly deviates from the earthquake hypocenters at intermediate depths (see Fig. 6). In general, we find the Slab1 model to be more consistent with the global ISC-EHB earthquake catalog for slabs in the wPac (Tonga, Japan Kuriles). However, the Slab2 model covers the ePac slabs in significantly more detail than Slab1. In particular, the Slab2 model seems to better capture the extent of slab flattening in Peru and partial slab flattening in Chile, relative to the older Slab1 model (for example, as shown in Fig. 9). This partial flattening of the northern Chile slab is well constrained by earthquake hypocenters as has been discussed in a number of previous studies Engdahl, van der Hilst, and Buland (1998); Fujita and Kanamori (1981b); Sippl, Schurr, Asch, and Kummerow (2018), and is important to our analysis.

In examining the relationships between between slab dynamics and geometry, we will refer frequently to the slab midplane. We use this term in relation to both the numerical model and observed slab geometries. The notion of a midplane serves as a proxy for the neutral plane of bending, and hence provides a way of analysing slab dynamics in terms of thin viscous sheet relationships (which are discussed in Section 5). Of course, the actual neutral plane of bending is a dynamic feature which may vary with respect to a fixed reference position such as the slab surface. However, for our purposes, knowledge of such variability is not essential. The analysis of the numerical model in Section

237   5, which is based on a slab surface referenced midplane, shows this approximation to the

238   neutral plane is sufficient for understanding the key relationships between geometry and

239   slab deformation rate. We generate a midplane by an orthogonal translation of the slab

240   surface model, with a distance that is proportional to thermal thickness of the plate at

241   the trench. We use a constant of proportionality of 0.2, consistent with estimates of how

242   DSZ width increases with plate age (Brudzinski et al., 2007). The resulting slab mid-

243   plane is illustrated in cross sections with dashed black lines (e.g. Fig. 6). Our analysis

244   requires knowledge of the slab geometry and its downdip gradients. In estimating the

245   curvature and curvature gradient of the midplane, a second order Butterworth filter is

246   used to remove short wavelengths of less than about 100 km.

2.2 Earthquake data

248   The accuracy of teleseismic-determined hypocenters varies considerably with lo-

249   cation technique, seismograph distribution, and hypocenter depth (e.g. Craig, 2019; En-

250   gdahl et al., 1998; Jackson, 1980). The approach we take to integrating available global

251   earthquake datasets is informed by several factors: 1) if only teleseismic P and S wave

252   travel times are used, depth errors may be several tens of km, due to fact that the ori-

253   gin time of an earthquake trades off against its focal depth (Jackson, 1980); 2) the use

254   of depth phases means that depth uncertainty can be reduced to around 10-15 km, sim-

255   ilar to epicentral uncertainties (Engdahl et al., 1998); 3) for shallow earthquakes (< 50

256   km), where the depth phases overlap with P wave coda, agency-reported depth phases

257   are likely to be less accurate (Engdahl et al., 1998); 4) depth errors in the CMT database

258   can be significantly higher than the best available global travel time data (Craig, 2019).

259   A simple way of addressing these issues is to combine the comprehensive CMT mo-

260   ment tensor database (Ekström, Nettles, & Dziewoński, 2012) with the hypocenters from

261   the ISC-EHB database. The ISC-EHB location procedure uses depth phases, via the EHB

262   algorithm (Engdahl et al., 1998), to minimise uncertainties in depth. In this study we

263   only consider the subset of events that are contained in both the CMT and ISC-EHB

264   catalogs, using moment tensor data from the former and hypocenter information from

265   the latter. Completeness magnitudes for the combined dataset will be limited by CMT

266   catalogue, which contains fewer small earthquakes than ISC-EHB. From 1976 - 2004 the

267   CMT catalog was complete to 5.4, while in the period following 2004 this was reduced

268   to Mw 5.0 (Ekström et al., 2012).

3 Methods

3.1 Megathrust event filter methodology

Earthquakes on the subduction megathrust constitute a very significant proportion of the overall seismic activity in shallow part of subduction zones. Although megathrust seismicity does not overlap spatially with intermediate depth earthquakes *sensu stricto* (> 70 km), filtering of potential megathrust events is extremely important in terms of identifying intraslab seismicity at shallow depths beneath the fore-arc wedge. Even with improved ISC-EHB locations, the depth uncertainties mean the use of hypocenter location data alone does not allow unambiguous discrimination of megathrust and intraslab events. Below we outline a procedure that combines both a seismic moment tensor similarity and hypocenter location to filter megathrust events from intraslab events.

We use the trench azimuth to define the strike and rake of the reference megathrust rupture tensor ($\mathbf{M}^{\text{ref}}$), assuming a pure double-couple mechanism, with the slab dip is set to 20° close to the average observed dip beneath the fore-arc in the regions considered here. The similarity measure (χ) of a given earthquake with ($\mathbf{M}^k$) is measured using the tensor dot product (:) of the normalised moment tensors:

$$\chi = \left[\frac{\mathbf{M}^{\text{ref}}_{ij} : \mathbf{M}^k_{ij}}{|\mathbf{M}^{\text{ref}}||\mathbf{M}^k|} \right] \tag{1}$$

We assume an event is a megathrust rupture if it has a recorded depth is less than 70 km, the hypocenter lies within 20 km of the Slab2 surface model and the moment tensor exhibits strong similarity to a reference megathrust rupture along the local part of the trench. We identify megathrust events using a focal mechanism similarity condition of $\chi \geq 0.75$. Fig. 1 show results from the application of this procedure along the Chile subduction zone. We focus in this region because it allows comparison with the recent publication of waveform-constrained hypocenters (Craig (2019), referred to here as Craig19). We note that the Craig19 data spans a shorter time interval than the ISC-EHB catalog, and is limited in its spatial extent, which means that the union of the CMT events and the Craig19 hypocenters yields a much smaller dataset than the union of CMT and ISC-EHB. Fig 1 shows the T-axes of identified as megathrust ruptures (black/grey) and intraslab events (orange). The T-axes are represented as projections of a uniform length vector onto a vertical great-circle plane. The identified megathrust events define a set

of nearly-parallel T-axes, with the highest density of hypocenters being between 15 and 40 km depth.

Because the majority of shallow subduction events in the catalog identify as megathrust events in this procedure (see Fig. 2d), even a relative small set of misidentified events could induce biases in our analysis. Our procedure could lead to such misidentification if there are a significant number of megathrust events with atypical rupture, or if there are significant numbers of proximal intraslab earthquakes with ruptures that are similar to our reference megathrust source. To further assess this possibility, Fig. 2 shows statistical distributions for spatial and source-related features of the data in Chile. The histogram in Fig. 2d shows the value of the normalised tensor similarity and emphasises that the majority of events show a high correlation with the expected slip on a megathrust, with the largest bin being the highest similarity. This does not rule out the possibility that we may exclude some megathrust events with atypical rupture mechanisms, it suggests that the basic assumption about homogeneity of megathrust sources is valid. Moreover, Fig. 2d shows that the chosen similarity value of 0.75 is meaningful in terms of distribution of earthquake orientation, as it represents the transition from the relatively flat part of the histogram, to the region where the histogram rises steeply at high moment tensor similarity associated with megathrust ruptures.

Fig. 2a shows the T-axes of the CMT moment tensor in a slab surface (Slab2) reference frame (as usual based on the ISC-EHB hypocenters). The vertical axis shows the distance of the earthquake hypocenter to the slab surface, while the horizontal axis shows distance along the slab surface. Histograms show the depth distribution (relative to the slab surface) for the two earthquake groups (i.e., megathrust and intraslab) shown in Fig. 1.The rotated T-axes of megathrust earthquake identified in our procedure share a characteristic orientation, plunging landward at close to 45° relative to the slab (Fig. 2a). The spatial distribution of identified megathrust events has a mean very close to zero (as shown with horizontal solid black line) and a standard deviation of about 6.5 km. The normal distribution corresponding to the same mean and standard deviation values is shown with black dashed lines in Fig 2a. The distribution is consistent with the idea that the typical maximum depth errors value have a value of 10 - 15 km (Engdahl et al., 1998). In practice we use a window of 20 km to capture megathrust events towards the tail of the distribution, which is important because of unequal population sizes (i.e. numbers of megathrust versus slab events). The distribution of identified megathrust earth-

331 quake is close to symmetric around the mean, consistent with the expected errors inher-
332 ent in depth-origin time trade off, although a slightly larger number of megathrust group
333 events lie in the lower half of the spatial window than in the the upper half (Fig. 2a).
334 This may indicate misidentification of some intraslab events. The orange histogram re-
335 flects the spatial distribution of events identified as intraslab earthquakes relative to the
336 slab surface (only events shallower than 70 km are shown). The mean of these events
337 is shown with the solid orange line, and lies at about 10 km below the slab surface. The
338 distribution of the slab earthquakes is weakly bimodal, with a peaks at around 8 km and
339 20 km consistent with existence of a DSZ.

340   Fig 2c shows the same filtering applied to hypocenters in the Craig19 study. In this
341 case, the events identified as megathrust ruptures are more compactly distributed, with
342 a standard deviation of 4.6 km. As noted in (Craig, 2019), the mean of the megathrust
343 events is systematically shallower than the Slab2 surface, by around 5km. Three iden-
344 tified megathrust events shown in Fig 2c lie more than 10 km from the mean value of
345 the set, and may represent slab earthquakes with megathrust-like rupture mechanisms.
346 As with the ISC-EHB data there a bimodal depth distribution for the intraslab group,
347 with peaks at similar spacing, although deeper by a few kilometres, compared to the ISC-
348 EHB data. Fig 2b compares the depth estimate for candidate megathrust events listed
349 in both ISC-EHB and Craig19 after subtracting the mean value of the offset relative to
350 the slab surface. The resulting difference in the depths between the 2 catalogs is up to
351 18 km, similar to the window width used (20 km) to identify potential megathrust events.

352   In addition to filtering megathrust events, all events with hypocentral depths more
353 than 20 km above the Slab2 surface are assumed to be upper plate events and are ex-
354 cluded from our analysis. While this is consistent with the inferred depth error distri-
355 bution for shallow earthquakes, it allows that some shallow forearc events may be erro-
356 neously identified as intraslab earthquakes. We think that the inclusion of forearc events
357 is relatively minor issue in most regions considered here. The interval post-Tohuku earth-
358 quake (2011) in Japan is an exception which we discuss specifically.

3.2 Numerical model

360   In Section 5 we discuss results from a numerical subduction model. The model was
361 developed using the Underworld2 code, and is closely based on setup described in D. San-
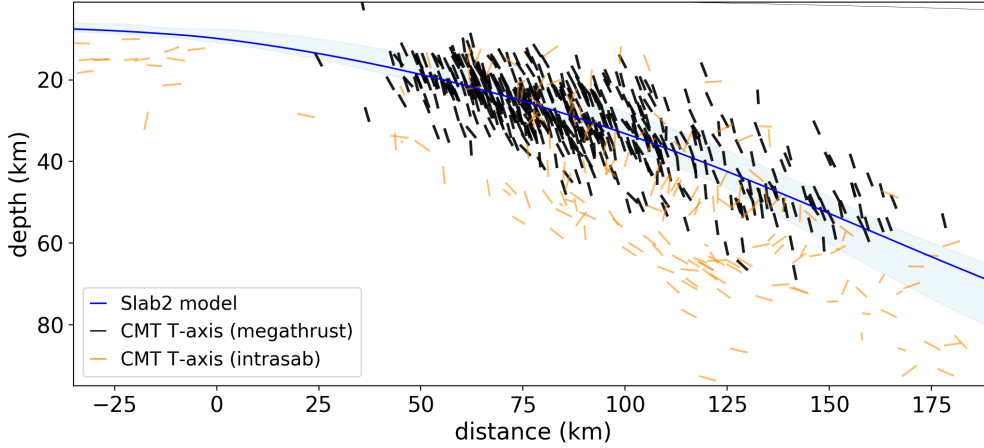
Figure 1. Distribution of filtered earthquakes in the near-trench zone (< 180 kms) in the Chilean region (Fig. 9 shows region bounds). Vectors represent CMT moment tensor T-axes, separated into inferred megathrust (black) and intraslab (yellow) events based on the similarity-procedure described in the main text. Hypocenters from the ISC-EHB Bulletin. Blue line shows the region-averaged Slab2 surface profile, while blue shaded region represents the variation of the Slab2 surface across the region.

diford and Moresi (2019). We refer readers to that study for a description of the governing equations, numerical method, model rheology, and implementation of the subduction interface. There are two significant changes in the setup of model described here: 1) we use a larger domain, with a higher relative resolution; 2) we constrain the upper viscosity limit in a small part of the mantle wedge to a value of 2×10^{20} Pa s. The geometry of the viscosity-limited region is shown in Fig. A.1 and constitutes an extremely simplified attempt to account for processes such as the presence of volatiles and melts in the wedge which are expected to substantially reduce the effective viscosity compared to dry, melt-free conditions. In terms of the model evolution the viscosity limit applied to this region has the primary effect of allowing asymmetric subduction to proceed even when the slab dip angle becomes quite shallow. If we did not provide this upper limit on the viscosity, the shallow part of mantle wedge would increase in viscosity as the slab dip decreases, due to a reduction in temperature (e.g. England & Wilkins, 2004). This creates increased coupling with the upper plate, and a rapid feedback cycle that results in a breakdown of single-sided subduction in model simulations.
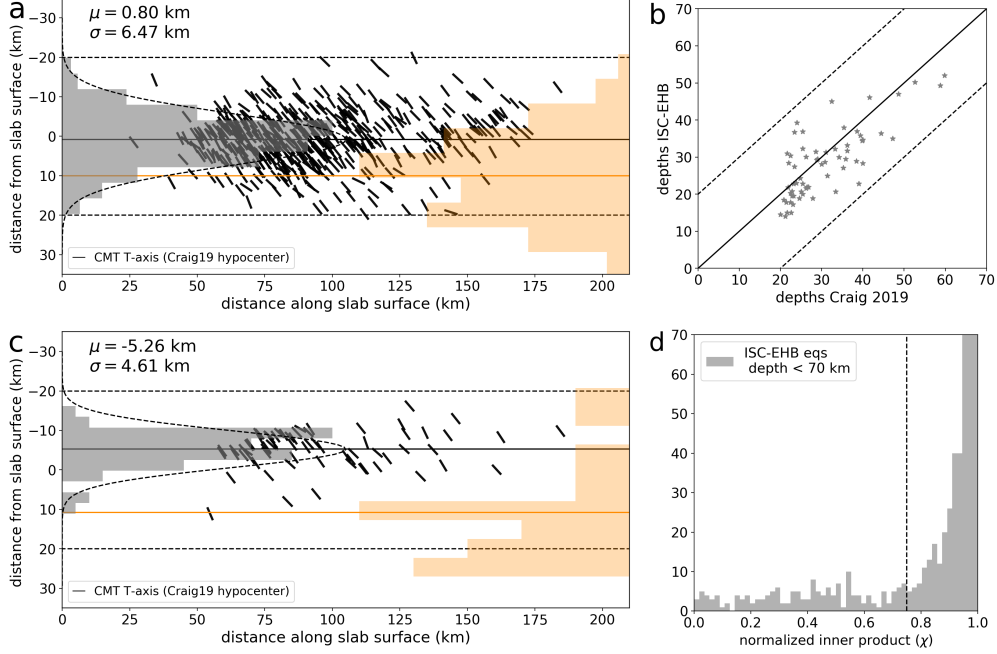
Figure 2. Statistical attributes of filtered earthquake locations in the near-trench zone for Chile region (see Fig. 9). a) CMT T-axes rotated into a slab-surface coordinate system, where the vertical axis is the distance from the slab surface, and the horizontal coordinate is the distance along the slab surface, relative to the location of the trench. Histograms show the distribution of the distance of the hypocenter (ISC-EHB) to the slab surface for megathrust events (grey) and intraslab events (yellow). Solid horizontal lines show the mean of the distribution; c) as for above, with hypocenters taken instead from the catalog of Craig19 (Craig, 2019); b) comparison of depths for identified megathrust events that appear in both the ISC-EHB and Craig19 catalogs; d) Histogram shows the distribution of the moment tensor similarity (χ) for all events with depths less than 70 km. A similarity of $\chi = 1$ implies the moment tensor is identical to the reference megathrust event. Vertical dashed line shows the limiting similarity value ($\chi = 0.75$) used in to filter megathrust events.

Fig. 15 shows a schematic of the model domain, including the initial conditions, boundary conditions, and evolution of the slab morphology during the simulation. Additional information about the numerical model setup is contained in Appendix A.

## 4 Study regions and seismicity

4.1 Western Pacific (wPac) seismicity

We consider three wPac slab segments: Tonga, Japan (northern Honshu), and the Kuriles. The domain limits are shown in Figs. 3, 4 and 5, along with cross sections providing a regional overview of slab seismicity. We have included deep (> 300 km) seismicity in these images, although our analysis is restricted to earthquakes shallower than 300 km. The coloured points show earthquakes designated as intraslab events. Earthquakes that lie more that 20 km above the slab surface (in the slab normal direction) are shown as small black points in the domain overview figures (e.g. Fig. 3). This step in our processing is primarily intended to capture upper plate events, which we therefore exclude from our analysis. However because we have not limited this condition in terms of absolute depth, we also capture a small number of slab earthquakes. Such anomalous earthquake locations may indicate substantial outliers in the data, or places where the region-averaged slab model does not adequately capture local irregularities in slab morphology at depth. Because the along-strike morphology of slabs tends to become more variable with depth, the deviation in hypocenters from the model slab geometry also tends to increase with depth. This accounts, for instance, for the large number of outliers in Tonga at depths > 300 km. Importantly, however, the region-averaged slab surface geometries provide a generally consistent fit to slab seismicity in wPac slabs at depths less than 300 km.

In Figs. 6-8 we highlight the orientation of slab earthquake moment tensors in the wPac slabs. The T-axes of the CMT moment tensors are plotted as projected vectors onto trench-perpendicular vertical planes (plane azimuths are shown on the region maps, e.g. Fig. 3). The length variation in the plotted T-axes reflects the magnitude of the projected component of the vector. That most of the T-Axes in the figures tend to have a similar length is a reflection that the least/most extensive eigenvectors of earthquake moment tensors tend to point downdip in slabs (Isacks & Molnar, 1971). The T-axes are expected to lie within the same quadrant as the smallest stress eigenvector. A common
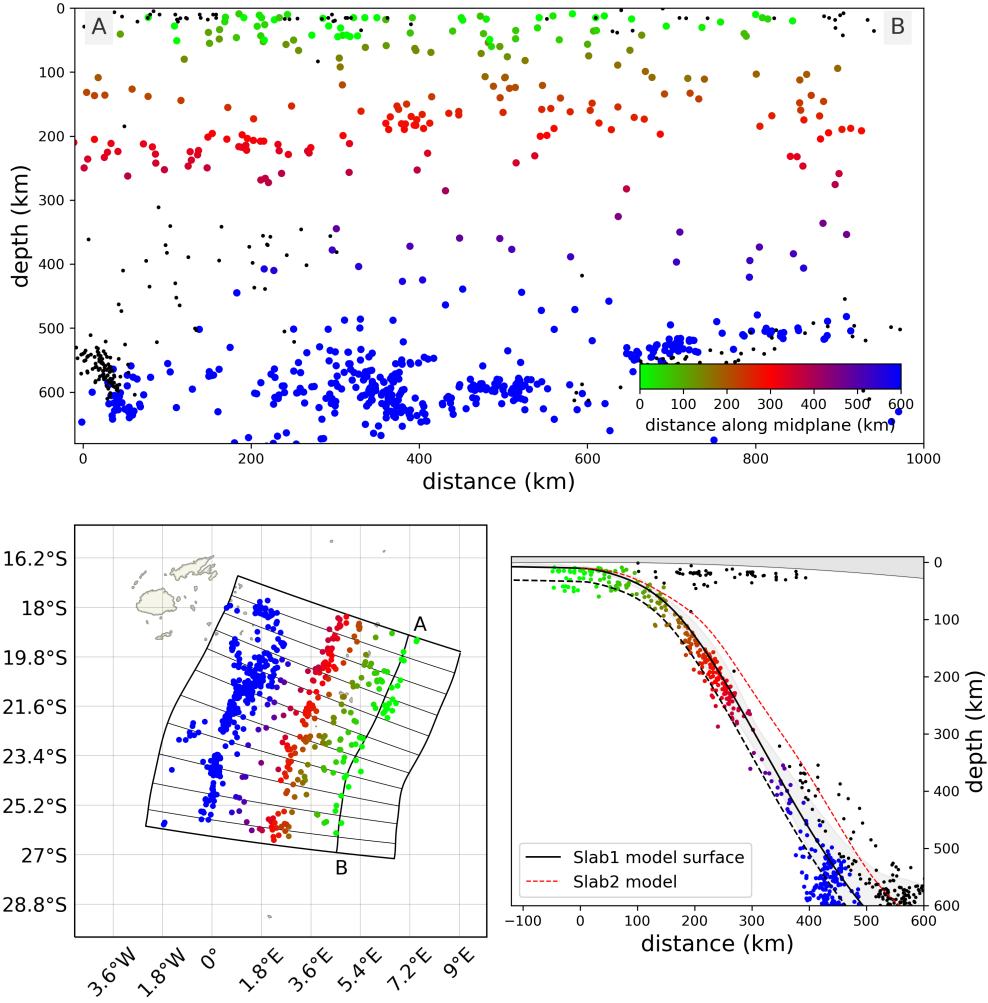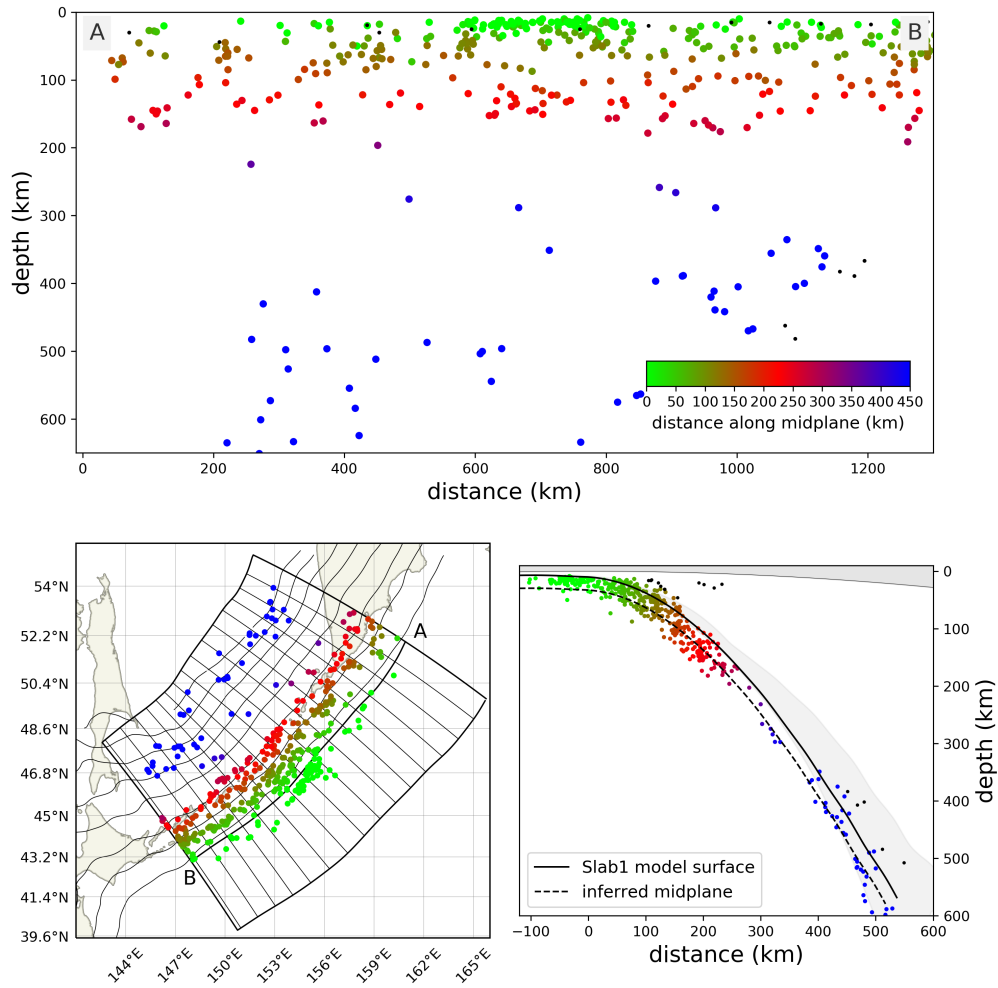
Figure 3. Overview of Tonga slab analysis region. Colored points show intraslab seismicity which is consistent with best available slab geometry model (Slab1 is used for Tonga region). Earthquakes lying more that 20 km above the slab surface are shown as small black points. We don't include these events in our analysis, as they can either be considered upper-plate events, outliers (presumably due to depth error), or regions where our slab models do not properly resolve the local slab morphology. Earthquakes identified as likely megathrust ruptures are excluded in these figures. The upper panel shows earthquakes projected on a great-circle plane lying parallel to the trench at the mid-point of the domain. Lower-left figure shows slab earthquakes in map view. Lower-right panel shows projection of the earthquakes on a trench-parallel cross section: the solid black line shows the region-averaged slab surface model; the gray region shows the variation in slab surface across the domain; the dashed black line shows the slab midplane (an orthogonal translation of the slab surface, as discussed in the main text); the red dashed line shows the Slab2 model for Tonga, which shows much less consistency with the earthquake hypocenters (ISC-EHB catalog).
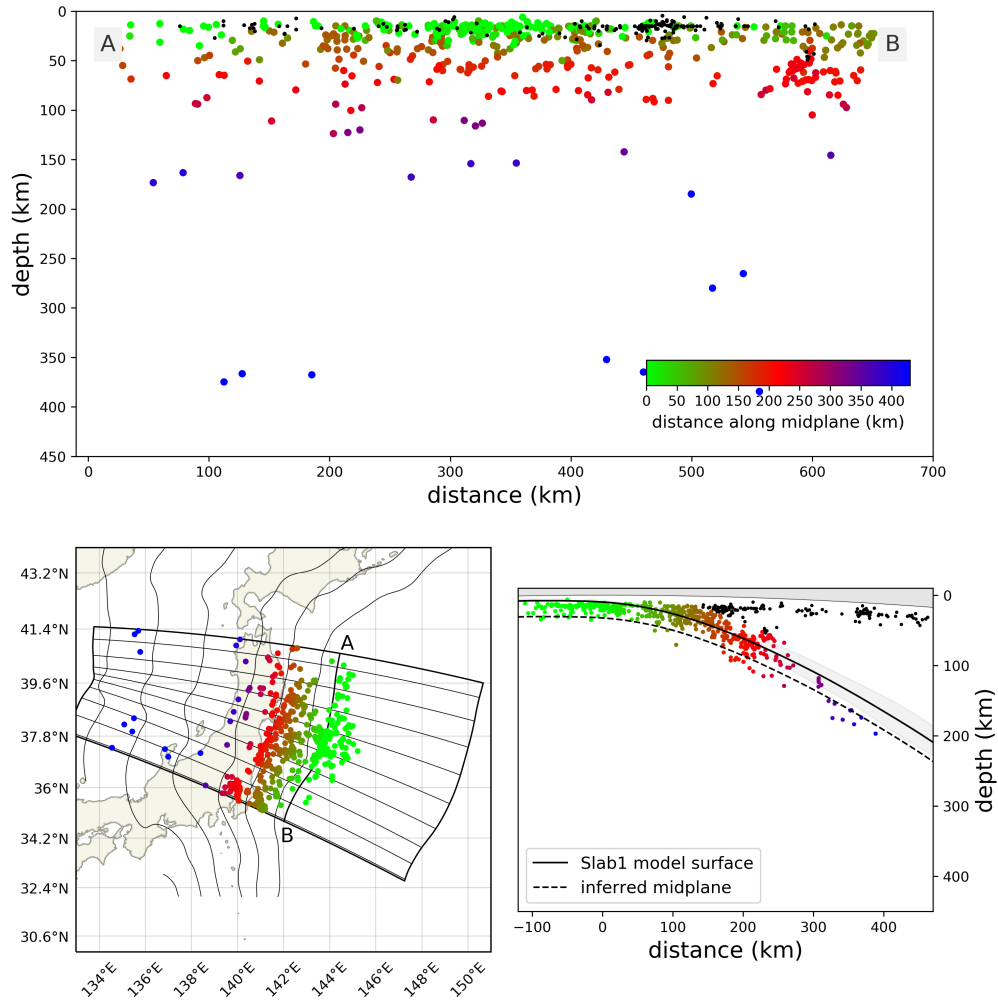
Figure 4. Overview of Japan slab analysis region. See Fig. 3 caption for details of figure organisation and preparation.

Figure 5. Overview of Kuriles slab analysis region. See Fig. 3 caption for details of figure organisation and preparation.

interpretation is that T-axes represent the orientation of most extensive co-seismic strain release (Bailey et al., 2009; Isacks & Molnar, 1971; Yang, Gurnis, & Zhan, 2017). The color of the T-axes represents the angle relative to the local slab orientation. Red axes show earthquakes with a DC sense, and blue axes those with a DT sense.

Outer Bending Zone (OBZ) events are evident in all wPac slab settings, typically starting at a distance between 50-120 km outboard of the trench. The fact that bending contributes to the stress-state in the outer-rise region is relatively uncontroversial (Chapple & Forsyth, 1979; Craig, Copley, & Jackson, 2014). In the wPac slab regions considered here, OBZ earthquakes cluster outboard of the peak in slab curvature which occurs landward of the trench (see also Figs. 17-19 and discussion in Section 6).

Historically, the role of unbending in slab seismicity has mainly been investigated in relation to Pacific Plate subduction (i.e. Kuriles, Japan, Tonga, Aleutians, and northern Marianas) (Engdahl & Scholz, 1977; Hasegawa et al., 1978; Kawakatsu, 1986a, 1986b; Samowitz & Forsyth, 1981; Tsukahara, 1980; Wang, 2002). The key observation is that these regions have DSZs which exhibit a characteristic 'polarity' switch in moment tensor between the upper and lower bands, characterised by DC and DT events, respectively. This distribution is very clear in the Kurile slab (Fig. 8) where a clear offset in the locus of DC and DT events occurs at depths between 70 - 200 km. The focal mechanism polarity switch, which is the defining feature of unbending-related DSZs, is also evident in both the Tonga and Japan slabs, although in both cases the relative number of lower plane DT to upper plane DC events is lower than in the Kuriles (e.g. Kawakatsu, 1986b). Importantly, while the PUZ in both Tonga and Japan is dominated by DC events, neither are exclusively DC (Figs. 6-8). As we discuss further below this is contrary to the expectation of uniform slab shortening of previous analyses (e.g. Fujita & Kanamori, 1981b; Isacks & Molnar, 1971; Richter, 1979).

At depths of around 60 - 200 km in the Japan slab, we see a clear indication of a polarised DSZ. Compared to the seismicity in the Kuriles and Tonga, the PUZ seismicity in the Japan slab is somewhat more clustered, particularly with regard to the distribution of lower plane DT events. We note that the great Tohoku megathrust event in 2011 impacted the Japan subduction zone during the catalog interval considered here. A result of the Tohoku earthquake is the appearance of a large cluster of extensional earthquakes in the shallow part of forearc (as labelled in Fig. 7), as discussed in previous stud-
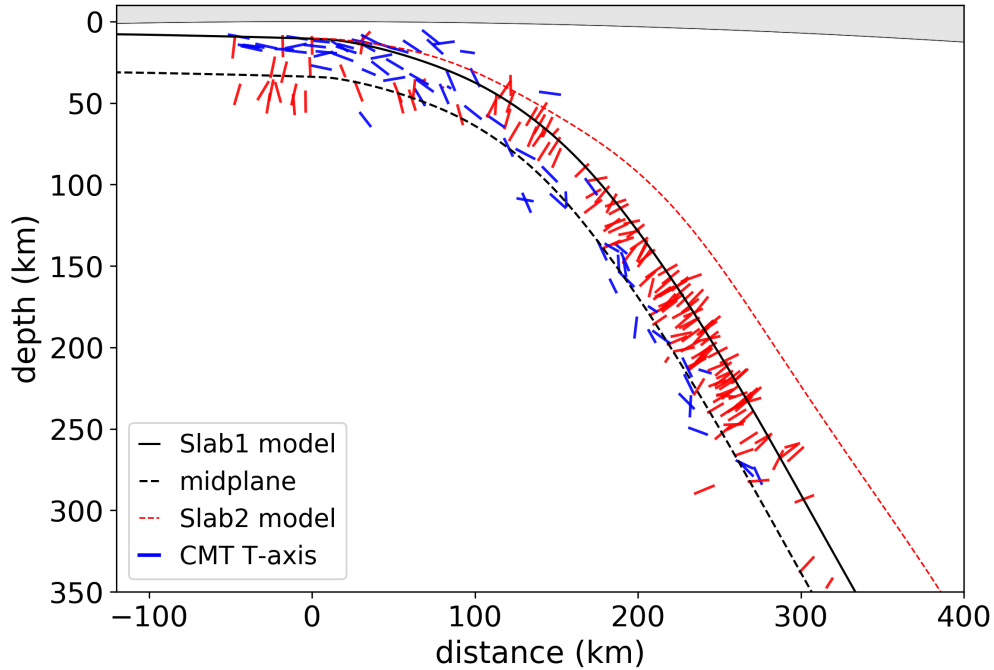
Figure 6. Tongan slab profile section. Projection of CMT T-axes (ISC-EHB hypocenters) on a vertical cross-section, along the azimuths shown with dashed lines in Fig. 3, with data aggregated across the entire domain. The T-axes are plotted as projections of uniform-length vectors, with the length variation in the plotted T-axes reflecting the magnitude of the projected component of the vector. T-axes are coloured according to the orientation relative to the slab midplane (shown with dashed black line): red represents earthquakes with a DC sense, blue with a DT sense.

440 ies (Imanishi, Ando, & Kuwahara, 2012). These events mainly lie within the 20 km win-
441 dow used to filter upper plate events, and are therefore misidentified as DT slab earth-
442 quakes. Supplementary Fig. B.1 shows the earthquakes in the catalog prior to 2011, where
443 the shallow forearc events are much fewer. The Tohuku earthquake also appears to have
444 influenced aspects of the intraslab earthquake distribution. For instance, a comparison
445 of Fig. 7) and Fig. B.1 suggests that unusually high levels of OBZ earthquakes have oc-
446 curred in the ~ 8 yrs since Tohuku. Interestingly, it appears that the number of unbend-
447 ing (PUZ) events in the has not increased in a comparable way, suggesting that stress
448 changes associated with the megathrust rupture have not influenced the deeper parts of
449 the slab as significantly as the incoming plate.
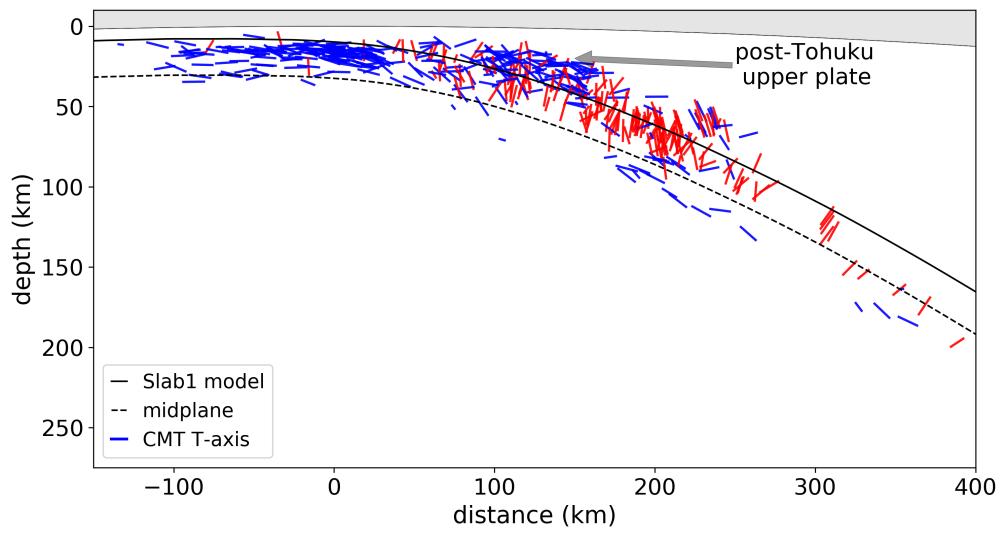
Figure 7. Japanese slab profile section. See Fig. 6 caption for details of figure organisation and preparation.
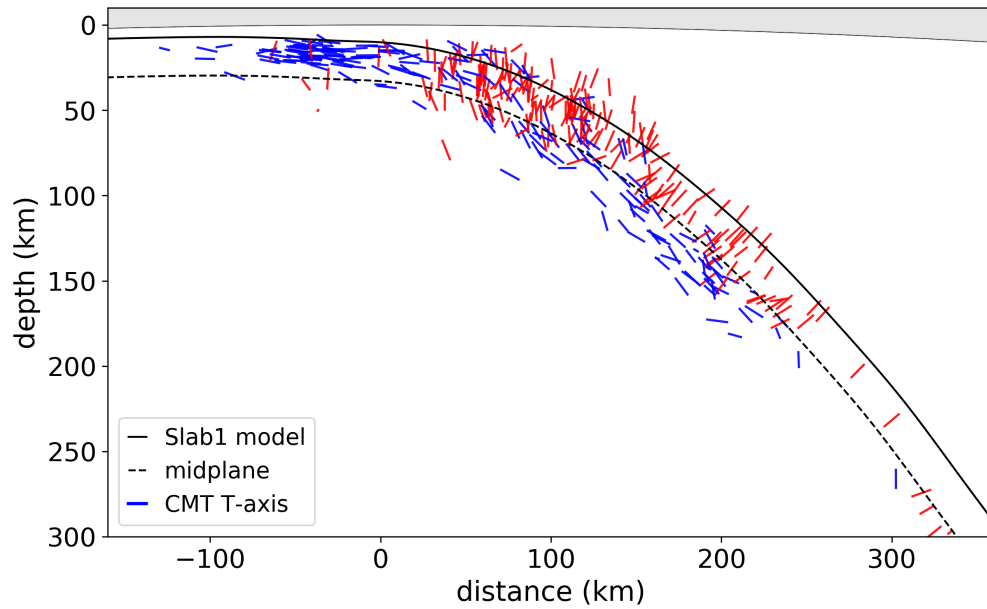
Figure 8. Kuriles slab profile section. See Fig. 6 caption for details of figure organisation and preparation.

4.2 Eastern Pacific (ePac) seismicity

Along the ePac margin we consider slab segments in Chile, Peru and Central America. The location of the regions are shown in Figs. 9 - 11, along with cross sections providing a regional overview of slab seismicity. As we have already discussed, the along-strike morphology of the ePac at intermediate depths slabs shows a greater degree of variability than is typical of wPac slabs. The presence of a number of prominent flat slab segments, such as Chile (Pampean), Peru and Mexico, is a reflective of this variability. This means that in addition to the ubiquitous presence of both OBZ and PUZ, ePac slabs commonly exhibit additional zones of bending and unbending.

Due to relatively low rates of seismicity OBZ and PUZ, resolving the seismic expression in the ePac slabs requires aggregating earthquakes across a significant distance along slab strike ($\sim$ 1000 km). Because the slab morphology is relatively coherent at these shallow depths, the analysis of aggregated earthquakes (and slab geometry) in the OBZ and PUZ is straightforward. However, with increasing downdip distance this coherence degrades. One implication is that a single 'region averaged' slab geometry is less capable of representing full variation in slab morphology, along with the range of seismicity contained therein. These issues are most significant in the case of Chile, which warrants some further discussion.

The Chile region, shown in Fig. 9, extends from the Bolivian Orocline in the north, to south of the Pampean flat slab. Within this region significant variation in slab morphology occurs, mainly associated with the Pampean flat slab, where the Juan Fernandez ridge subducts. Despite this variability, we treat the entire region as single domain. This takes advantage of the fact that: a) the width of the Pampean flat slab is relatively narrow with respect to the size of the domain, and b) the rates of intermediate dwpth seismicity in the Pampean slab very are low compared to the northern part of the Chile slab (i.e. the north Chile seismic belt, shown in Fig. 9). Because of the skewed nature of seismic activity, the main contribution to the aggregated intermediate depth seismicity (i.e. when plotted in cross section) comes from northern Chile. Of course, if we were only interested in immediate depth seismicity (> 70 km), it would suffice to simply consider restricted region in the northern part of the domain. This would mean, however, that the seismic expression of the OBZ and PUZ would be less clearly defined. Hence, the cross section for Chile (Fig. 12) provides something of a dual perspective: with the

shallower seismicity (< 70 km) being reflective of region-wide seismic expression, while the intermediate depth seismicity is dominated by the north Chile seismic belt. Because the main contribution to the intermediate depth seismicity in Chile comes from the north Chile Seismic Belt, our geometric analysis (section 6) is based on a slab surface model that reflects the slab morphology in north.

OBZ earthquakes are evident in all ePac slab settings, reflected in normal faulting events in the upper part of lithosphere. When compared to the wPac settings discussed above, two differences stand out. In ePac the frequency of OBZ events is significantly lower, and the OBZ events tend to be clustered much closer to the trench. In Peru, the small number of OBZ events are all located within about 10 kms of the trench, with most of these in fact being slightly landward (Fig. 13).

Clusters of earthquakes at about 100 km inboard of the trench in Chile, and 150 km in Peru, provide evidence for the existence of unbending DSZs along the ePac margin (Figs. 12 - 13, see also Figs. 20 - 21 as discussed in Section 6). Both cases contain a band of dominantly DC events overlying a smaller group of DT events. As we will show in Section 6, these events occur in the region where inferred rates of slab unbending are highest (i.e. in the PUZ). Compared to the wPac, an important difference in the PUZ seismic expression is the relative depths at which they appear. Because the ePac unbending events occur at relatively shallow depths and spatially overlap with the megathrust zone, removing of the megathrust event is critical to their resolution. While the significance of ePac DC events in terms of a putative unbending DSZ, have been noted previously (e.g. Barazangi & Isacks, 1976) this interpretation has not previously gained much traction, and other studies have posited alternative interpretations, such as slab-push (Lemoine, Madariaga, & Campos, 2002), or flexural slip (Romeo & Álvarez-Gómez, 2018).

Downdip from the PUZ, the slab morphology in Chile and Peru deviates substantially. Peru has a very long ($\sim$ 300 km) flat slab region, followed by a steepening associated with a prominent peak in curvature at around 600 km from the trench (the distal hinge of the flat slab section). The trench normal view of Peruvian seismicity, shown in the upper panel of Fig. 10 is striking. Earthquakes in the flat slab form a belt, with an average depth of $\sim$120 km, over a distance extending more than 700 km along the trench, with a slight concave up distribution. A cluster of earthquakes, known as the Pucallpa seismic nest, forms a subset of these flat slab earthquakes, and are proximal to

514 a localised depression along the distal hinge of flat slab (Gutscher, Spakman, Bijwaard,

515 & Engdahl, 2000; Wagner & Okal, 2019). Our regionally averaged slab morphology clearly

516 does not captures this subtle variation. In Fig. 13 the Pucallpa events have been high-

517 lighted using a greater transparency level.

518 While the slab morphology for northern Chile, shown in Fig. 12, does not contain

519 a prominent flat slab *sensu stricto*, there is a subtle upwards deflection beginning at around

520 200 km from the trench indicative of partial flattening. While the profile section shows

521 this as a subtle feature, the implied curvature is quite sharp, as discussed further below.

522 In both Chile and Peru, slab seismicity at intermediate depths is dominated by DT

523 ruptures. In Peru, seismicity is distributed throughout the flat slab, becoming more fre-

524 quent towards the distal hinge. In Chile, the DT events evident in Fig. 12 are clustered

525 in two zones. The first of these overlaps with the zone of partial slab flattening, between

526 200 and 350 kms from the trench, centered at a depth of $\sim$ 110 km, and appear as red

527 points in Fig. 9. The second cluster is more diffuse, concentrated between 400 and 500

528 km from the trench, appearing as blue points in Fig. 9. When viewed in a trench-parallel

529 cross section (Fig. 9 upper panel), the two zones of intermediate depth DT seismicity

530 in Chile have quite different characteristics. This shallower zone forms a sub-horizontal

531 band of seismicity, which is most intense in the northern part of the domain (labelleled

532 the 'north Chile seismic belt') but is also evident in parts of the southern half of the do-

533 main. The deeper zone of DT seismicity has hypocenters which form a band oriented

534 at a relatively high angle to a horizontal plane (i.e. Fig. 9 upper panel). We have high-

535 lighted these earthquakes with a red dipping dashed line in Fig. 9. The framework pre-

536 sented in this study has applicability to the north Chile seismic belt, but not the deeper

537 earthquakes. The unusual distribution of this deeper cluster of earthquakes may indi-

538 cate a spatially and temporally localised process like slab tearing, whereas our study at-

539 tempts to highlight the signal of time-independent, geometric bending.

540 The patterns of seismicity in Central American slab are far less clear than the other

541 regions we consider in this study. For instance, the hypocenter locations shown in the

542 cross section (Fig. 14) exhibit substantial scatter at all depths, as well as less pronounced

543 downdip clustering than in Chile or Peru (where we argue that such clusters are asso-

544 ciated with different bending zones). One possibility is that the morphological variabil-

545 ity of the Central America slab, even at shallow depths, blurs the patterns in the aggre-

gated seismicity. In the Central American region, the case for a seismicity associated with a PUZ is not clear. While there are a number of events in the Central American slab which have a DC component (red axes in Fig. 14), and could potentially indicate unbending, there is no clear spatial separation between DC events and the more numerous DT earthquakes. Moreover, Fig. 14 shows that the principal-axes of the DC events, are not strictly aligned with the slab as is expected for unbending. It is possible that these DC events (red axes in Fig. 14) are deep, poorly located, megathrust ruptures, that have been misidentified in our filtering procedure.

The morphology of the slab in Central America is characterized by two distinct zones of steeping (based on the Slab2 geometry shown in Fig. 14). The slab unbends fully at about 100 km from the trench, before steepening again with a second peak in curvature at about 175 km from the trench. Unlike the other ePac settings we have discussed, no clear dip angle reduction takes place between these peaks in curvature. The majority of earthquakes in the Central American slab have DT ruptures, and are concentrated at a distance of about 130 km from the trench. As we show in Section 6, this places the majority of DT earthquakes in a zone of curvature increase where, similar to the outer rise, stretching of the upper part of the slab is expected. We must highlight, however, that the consistency between the seismicity and the slab surface model is relatively poor in Central America, and we therefore place less emphasis on results from this region.

5 Insights from numerical modeling

In this section we present results from a numerical subduction model, which serves primarily to highlight how different modes contribute to the overall slab deformation rate. The setup of the numerical model is very similar to the description in D. Sandiford and Moresi (2019), and more extensive details of the model are provided in Appendix 1. The flow is driven entirely by the thermal density contrast of the slab. Mantle rheology (including oceanic lithosphere) is prescribed by a composite flow law that includes linear high-temperature creep, as well as a scalar visco-plastic approach sufficient for capturing psuedo-brittle as well as distributed plastic deformation within the slab (see A for additional information). The model does not include any stored elastic stress component. This common simplification assumes that elastic stress is relaxed on a relatively short time/length scales.
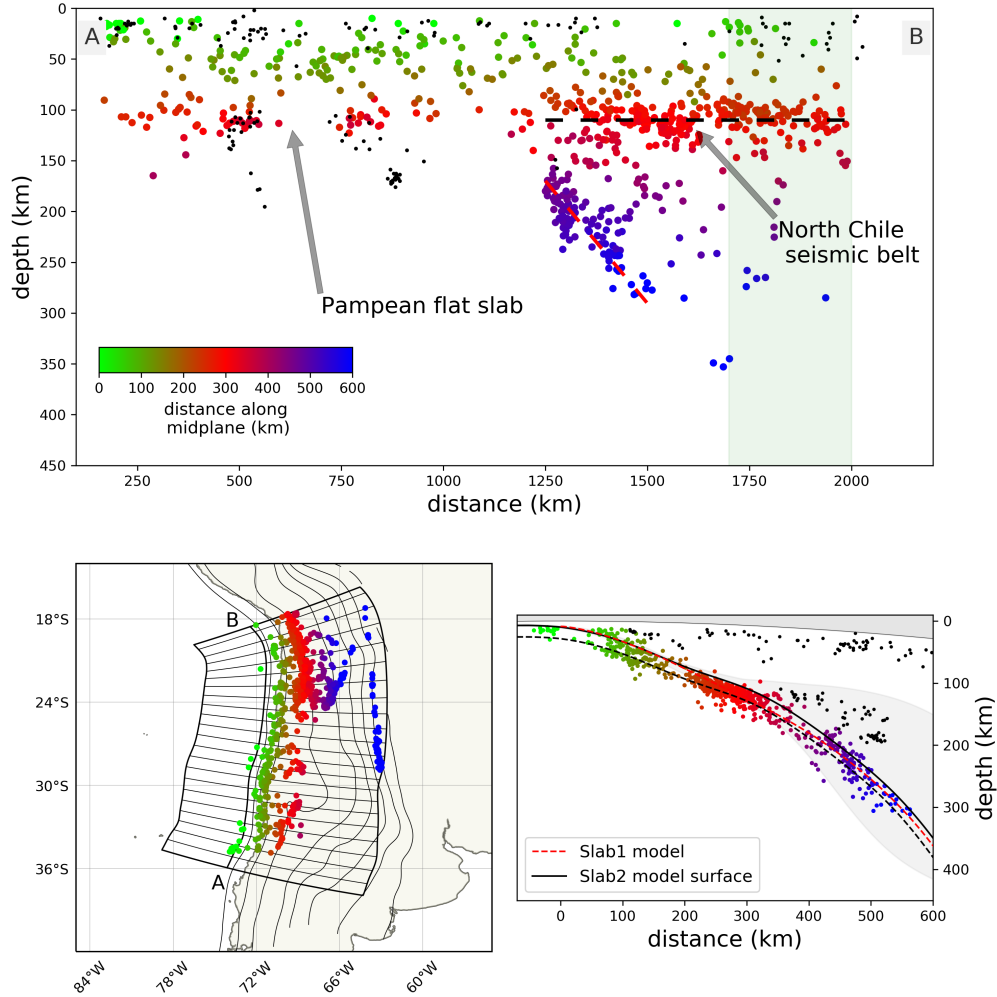
Figure 9. Overview of Chilean slab analysis region. See Fig. 3 caption for details of figure organisation and preparation. The black points represent earthquakes that lie more the 20 km above the slab surface model. These mainly represents the relatively small number of earthquakes that occur in close proximity to the Pampean flat slab in the south, where the slab morphology is quite different to northern Chile. The green band in the top panel corresponds to a restricted region which we plot in Fig. B.2.
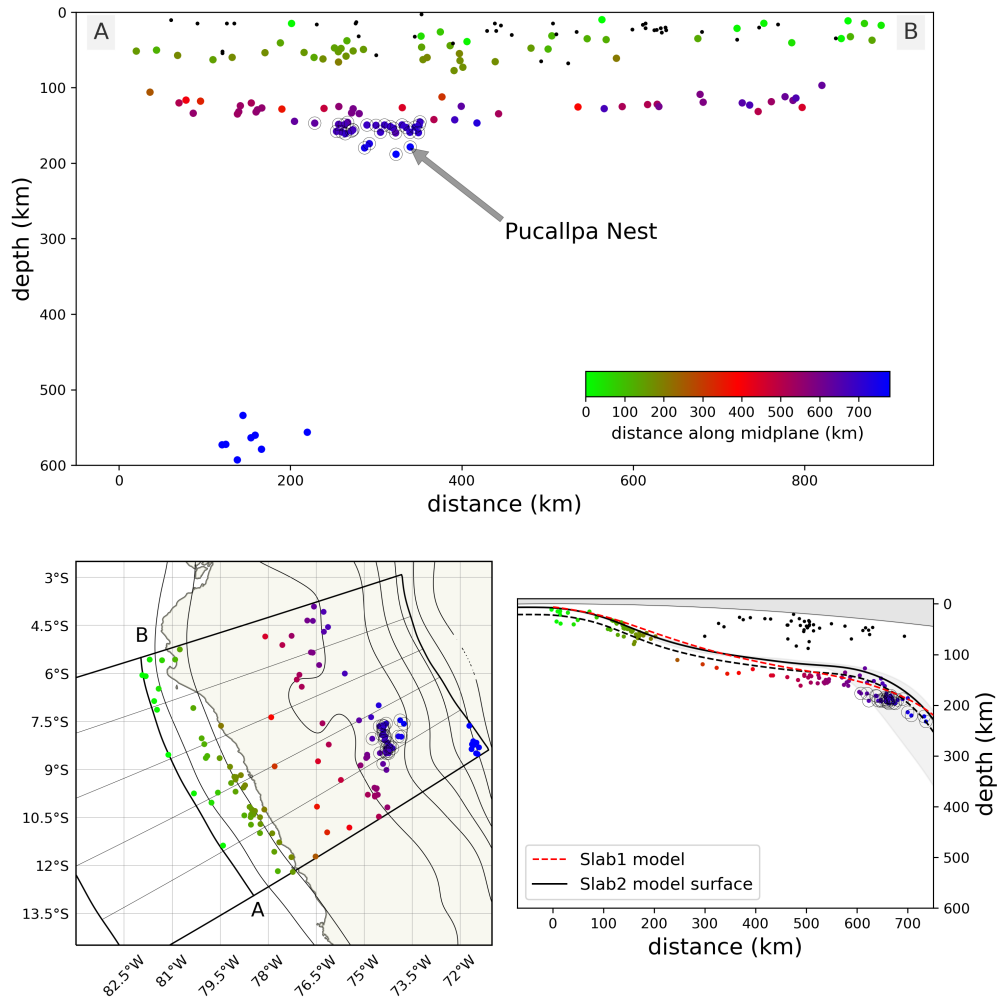
Figure 10. Overview of Peruvian slab analysis region. See Fig. 3 caption for details of figure organisation and preparation.
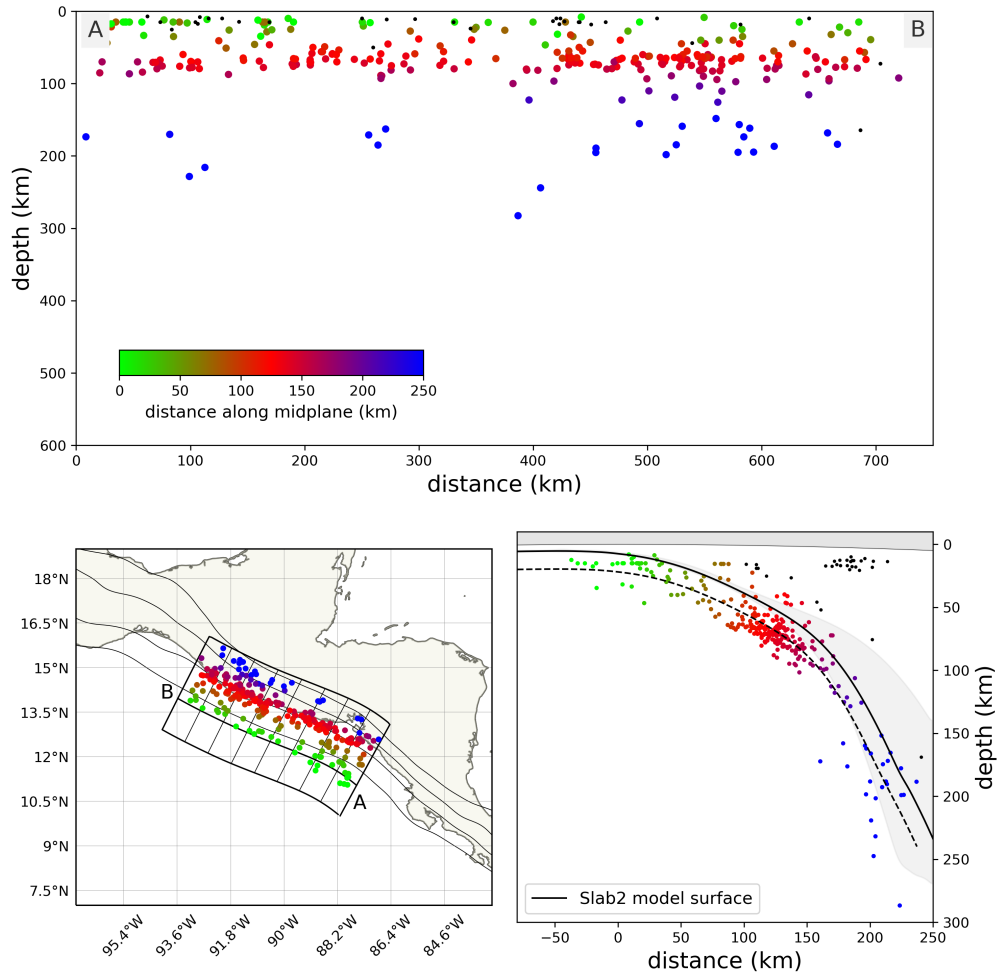
Figure 11. Overview of Central American slab analysis region. See Fig. 3 caption for details of figure organisation and preparation.
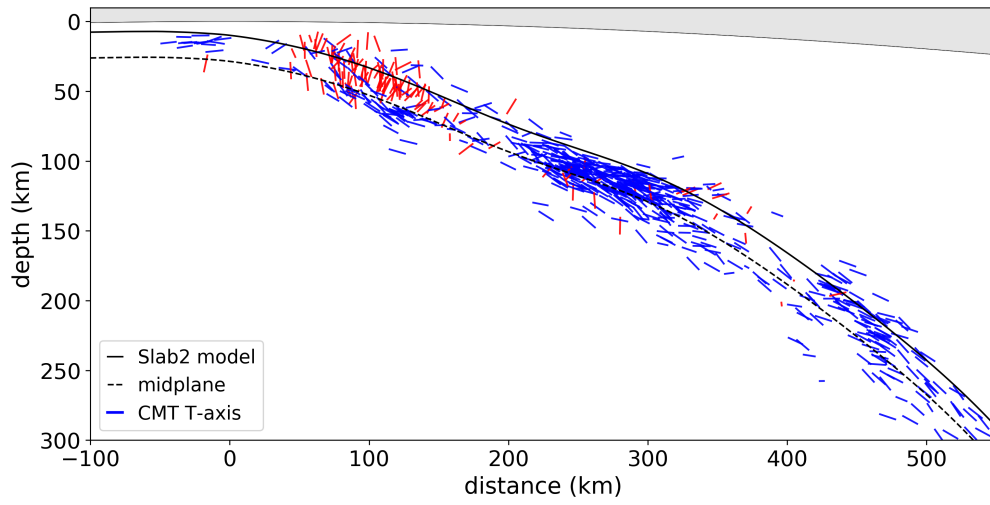
Figure 12. Chilean slab profile section. See Fig. 6 caption for details of figure organisation and preparation.
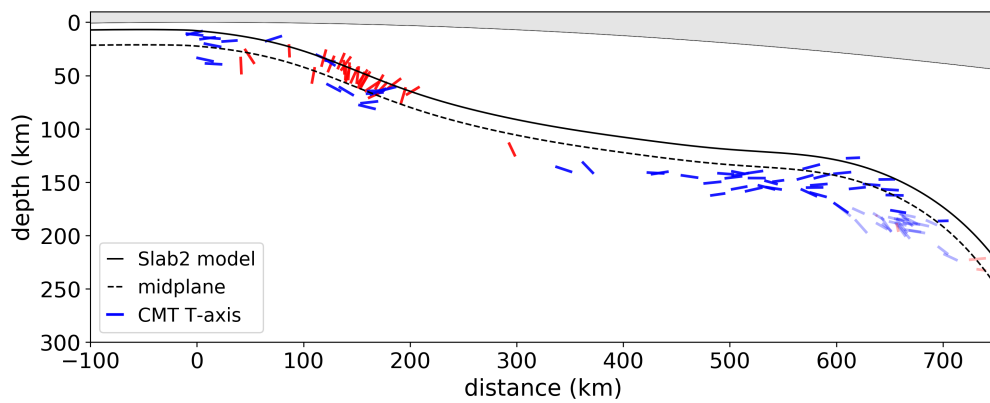
Figure 13. Peruvian slab profile section. See Fig. 6 caption for details of figure organisation and preparation.
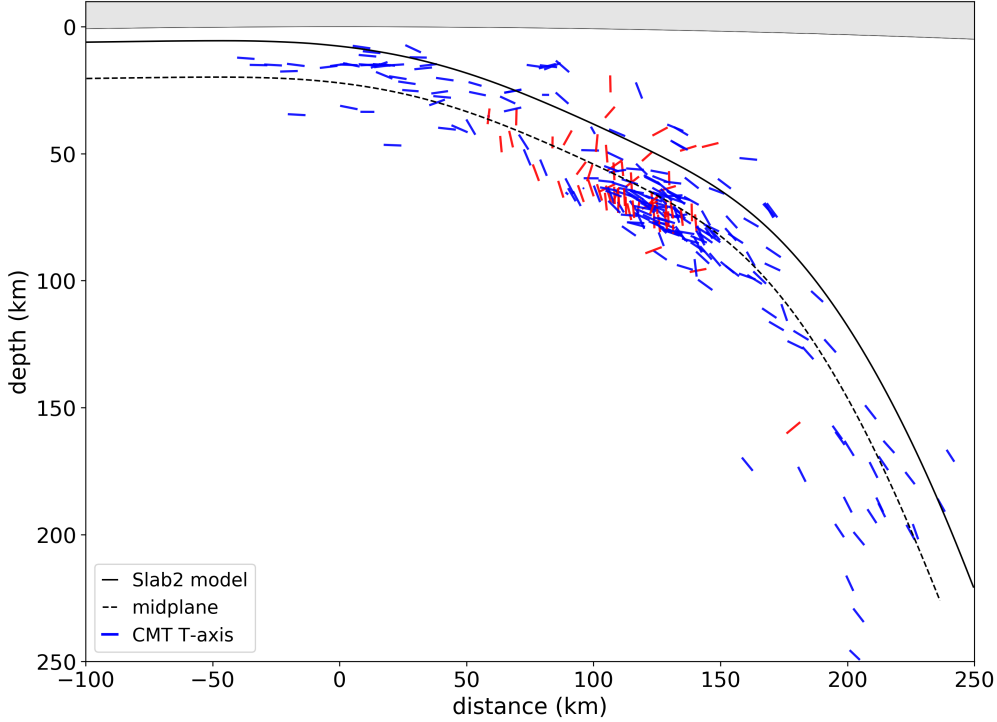
Figure 14. Central American slab profile section. See Fig. 6 caption for details of figure organisation and preparation.

In Fig. 16 we show the downdip component of the strain rate ($\dot{\epsilon}_{ss}$) at two time intervals, with the top panels in each figure showing the normalised value of curvature and curvature gradient evaluated along the slab midplane. The fact that flexural deformation dominates the downdip slab strain rate is apparent from observing that all regions of high strain rate are polarised, with shortening (red) on one side of the slab and stretching (blue) on the other. If uniform deformation modes were dominant, we would expect to see entire sections of slab undergoing stretching or shortening. It may seem surprising that a system which is driven entirely by slab buoyancy is not dominated by uniform stretching due to slab pull. This outcome is a consequence of the fact that nearly all of the slab pull force is balanced by drag in the mantle. This subduction style is often referred to as the Stokes regime (F. Capitanio, Morra, & Goes, 2007; Gerardi & Ribe, 2018; W. P. Schellart, 2004). In the inset axis of Fig. 16, at 10 Myr, we plot the stress in the subducting plate. The peak stress is on the order of 10 MPa. This is more than order of magnitude smaller that the stress that would be produced if a significant part of the

591 weight of the slab was connected to the plate (i.e. when the slab pull factor are *sim* 0.5(e.g.

592 Conrad & Lithgow-Bertelloni, 2004)).

593 The numerical model shows that flexural, rather than uniform deformation modes,

594 tend to dominate the subduction hinge in the Stokes regime. Another important insight

595 provided by the model relates to the strong geometric control on bending rates. When

596 a sheet is deformed by pure bending, the distribution of strain rate in the downdip di-

597 rection ($\dot{\epsilon}_{ss}$) is a function of the curvature rate (a material derivative) multiplied by dis-

598 tance from the midplane (Kawakatsu, 1986a; Ribe, 2001; Tsukahara, 1980):

$$\dot{\epsilon}_{ss} = -y\frac{DK}{Dt} = -y\left(\frac{\partial K}{\partial t} + u_s\frac{\partial K}{\partial s}\right) \tag{2}$$

599 where s refers to a unit vector along the slab midplane, y is the distance perpendicular

600 to the midplane, $\frac{D}{Dt}$ is the material derivative following s, K is the curvature and u_s is

601 the velocity component parallel to the midplane. The term $u_s\frac{\partial K}{\partial s}$ is sometimes referred

602 to as an advective bending rate; we will also use the term geometric bending to empha-

603 sise the the fact that it is the present day slab geometry that constrains this (time-independent)

604 component of the bending rates.

605 At both of the time intervals shown in the Fig. 16, we see a strong correlation be-

606 tween the curvature gradient profile ($\frac{\partial K}{\partial s}$) and the downdip strain rate distribution ($\dot{\epsilon}_{ss}$).

607 The zones where downdip strain rates are smallest coincide with the local maxima in the

608 curvature amplitude, where the curvature gradient is close to zero. This suggests that

609 the advective component of the bending rate is a dominant control on the both the to-

610 tal bending rate (as well as as the overall slab deformation rate). At 10 Myr, we see a

611 typical slab morphology, characterised by plate bending outboard of the trench (OBZ)

612 and slab unbending centered at around 70 km depth (PUZ). At 25 Myr, the slab has be-

613 gin to deflect upwards beneath the upper plate. This zone is associated with increasing

614 curvature (positive curvature gradient) which produces extension in the upper half the

615 slab and shortening in the lower half of the slab. The numerical model morphology at

616 25 Myr is reminiscent of the partial flattening of the Nazca slab in northern Chile (Fig.

617 12).

618 The distribution of slab temperature, relative to patterns of internal slab dynam-

619 ics, are important for thinking about which parts of the slab are likely to be seismogenic.

620 The brittle ductile transition in lithospheric mantle is thought to occur at a potential
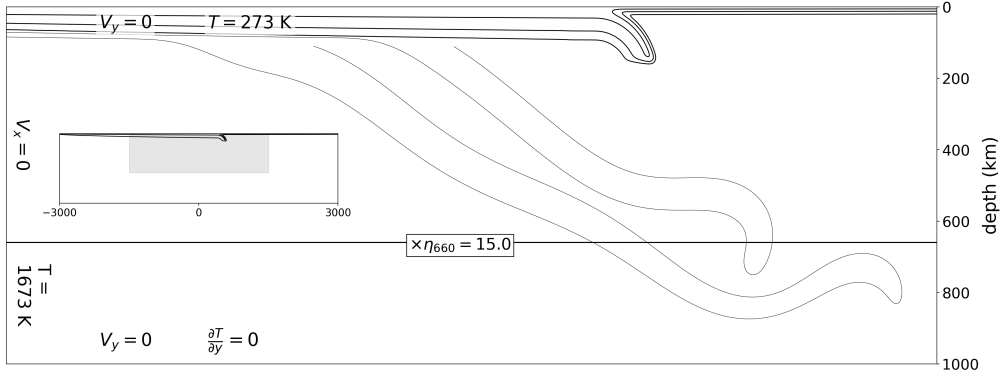
Figure 15. Numerical model setup. The main panel shows a restricted part of computational domain. Contours of the slab temperature show the evolution of the model at times 0, 10, 25 Myr. Inset panel shows the full computational domain (6000 km x 1500 km).

⁶²¹ temperature near 600 °C (Emmerson & McKenzie, 2007). In the model, a gradual re-

⁶²² duction in subduction velocity between 10 Myr and 25 Myr is a primary control on why

⁶²³ the depth of the 600 °C isotherm has reduced from about 300 km to less than 150 km

⁶²⁴ over that time interval. We note that in the numerical model, the 600 °C isotherm en-

⁶²⁵ closes the upper-half of each bending region: the simple prediction would be that strain

⁶²⁶ would only be released seismically in the upper half of the bending zones (i..e above the

⁶²⁷ neutral plane). In many of slab we discussed regions, however, we see the seismic expres-

⁶²⁸ sion of both halves of the bending region, even if that distribution is often asymmetric.

⁶²⁹ This points to a limitation in the subduction models, which should be kept in mind.

6 Seismicity geometry relationships

⁶³¹ In this section we assess the role of advective bending in relation to the seismic ex-

⁶³² pression of Pacific margin slabs. Within each slab region, the relative variation in the

⁶³³ advective bending rate is associated with downdip curvature gradient of the neutral plane,

⁶³⁴ according to the relationship in equation 2. We calculate curvature gradient using the

⁶³⁵ estimated slab midplane (a proxy for the neutral plane) as described in Section 2. The

⁶³⁶ visualisations we use to explore these seismicity geometry relationships differ somewhat

⁶³⁷ to those in Section 4. Here we plot the earthquake T-axes in a slab midplane coordinate

⁶³⁸ system, with distance from the hypocenter to the midplane shown on the vertical axis,

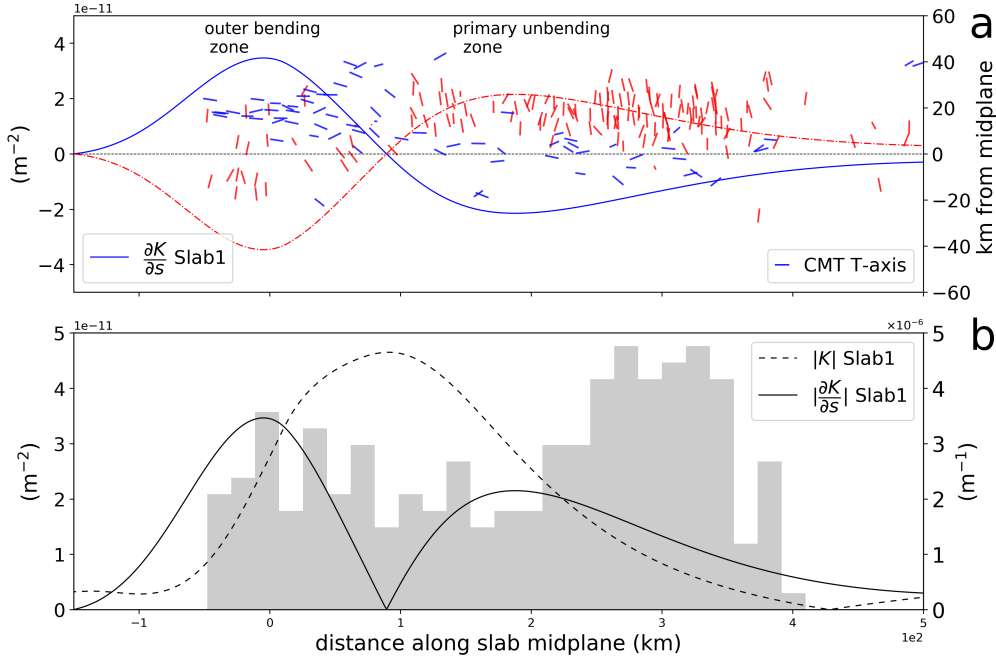⁶³⁹ and distance along the midplane relative to the trench (horizontal axes). As in the ear-
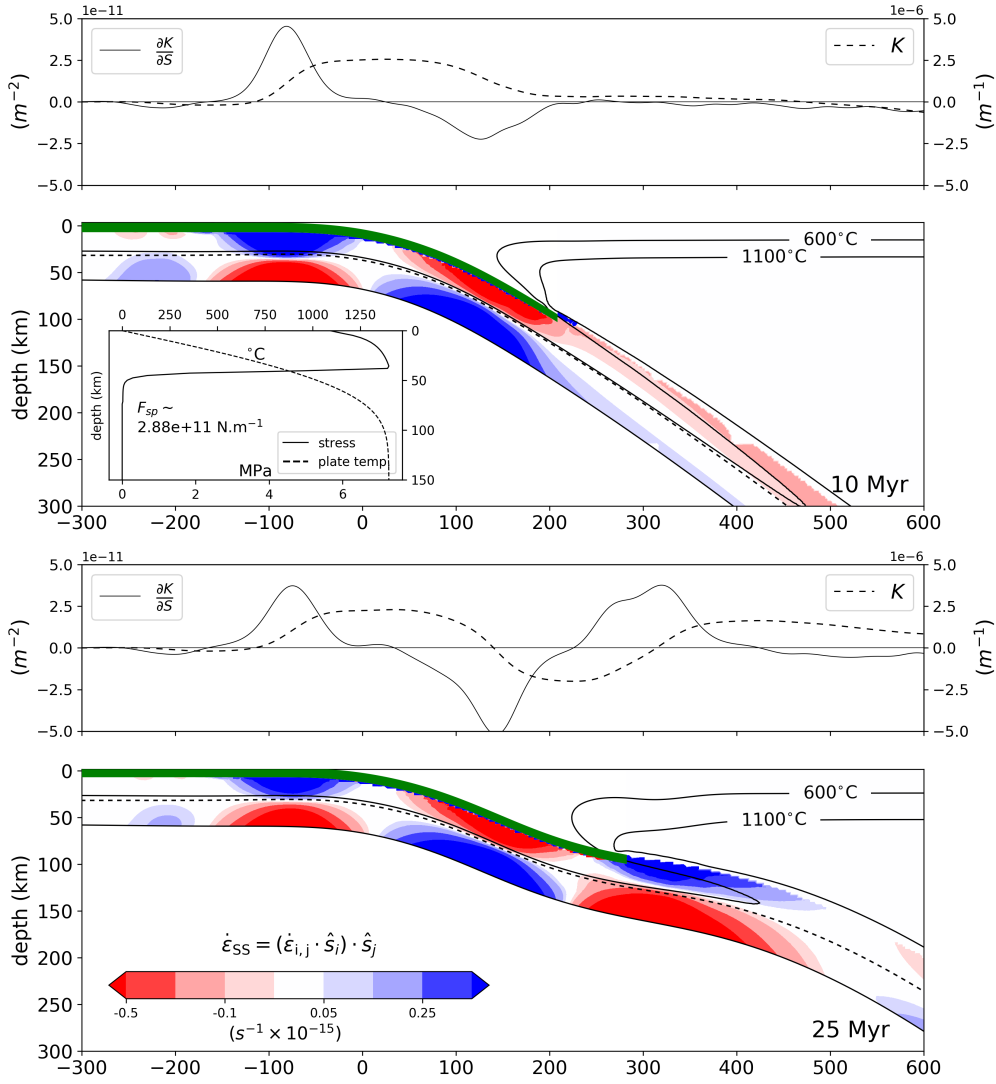
Figure 16. Strain rate distribution in numerical model at 10 Myr and 25 Myr. In each figure. The main panels show the downdip strain rate component in the slab ($\dot{\epsilon}_{ss}$) resolved parallel to the slab midplane. We show only the strong interior part of the slab: the subduction interface zone, upper plate, and parts of the mantle are above 1100°C isotherm have been masked. +ve values (blue) show zones of downdip extension, -ve values (red) are shortening. Solid black lines show isotherms as labelled. Dashed black line is the slab midplane. Shaded green region represents the subduction interface. Inset in the panel at time 10 Myr shows the temperature and stress (horizontal component) profile in the plate at 300 km to the LHS of the trench. The smaller upper panels shows the curvature and curvature gradient of slab midplane, plotted along the same horizontal axes as the main panels (distance from trench).

lier figures, the T-axes are projections on to a trench normal plane, but here they are rotated so that the angle relative to the midplane is preserved.
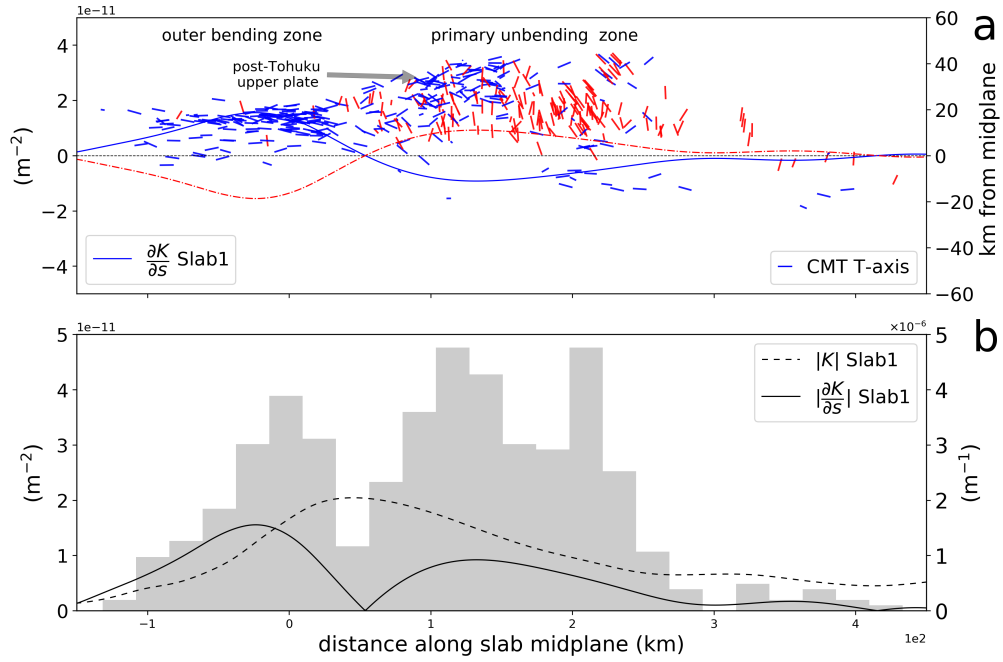
Figs. 17-19 show seismicity geometry relationships for the wPac regions. In the upper panel, we show the rotated T-axes. In the lower panels we show histograms representing the number of intra-slab earthquakes per unit distance along the midplane (note this is not equivalent to the total strain or moment release). Curvature and curvature gradient are plotted on the same horizontal axis (representing distance along the midplane) as indicated in figure legends. The curvature gradient profiles associated with wPac slabs reflect the relatively simple morphology of the slab hinge. In the plate bending region, curvature gradients show a relatively symmetric positive peak, with a half-wavelength of between 150 - 200 km. Peak curvature (zero gradient) occurs at a considerable distance (50 - 100 km) downdip from the trench. Beyond this, the downdip gradient changes sign and thereafter tends to decay monotonically as the slab straighten out in the mid upper mantle. In the wPac, OBZ earthquakes tend to center either near the peak in positive curvature gradient (e.g. Kuriles), or in between the peak in curvature gradient and the peak in curvature (e.g. Japan, Tonga), but not at the peak in curvature.

The point where the curvature gradient switches sign is generally coincident with the transition between the OBZ earthquakes (DT earthquakes above the midplane), and the DSZs that we interpret (following many others) as being related to unbending (i.e. the PUZ, with DC earthquakes above the midplane, DT beneath). This transition does not necessarily represent a sharp inversion in the orientation of T-axis. In the Kuriles, for instance, a zone of several tens of kms exists where T-axes are somewhat random, before the unbending DSZ emerges. In Japan, the transition to negative curvature gradient coincides with the onset of upper-plane DC seismicity, but the onset of lower plane DT events does not appear to commence until about 100 km downdip of the transition. Clearly there are complexities in the relative number of upper plan (DC) and lower plane (DT) events, as evidenced by the strong asymmetry we see in the Tonga DSZ, versus much more symmetrical distribution in the Kuriles. Nevertheless, the orientation of seismicity in wPac slabs - particularly the upper plane seismicity - varies in a systematic way with the slab curvature gradient.
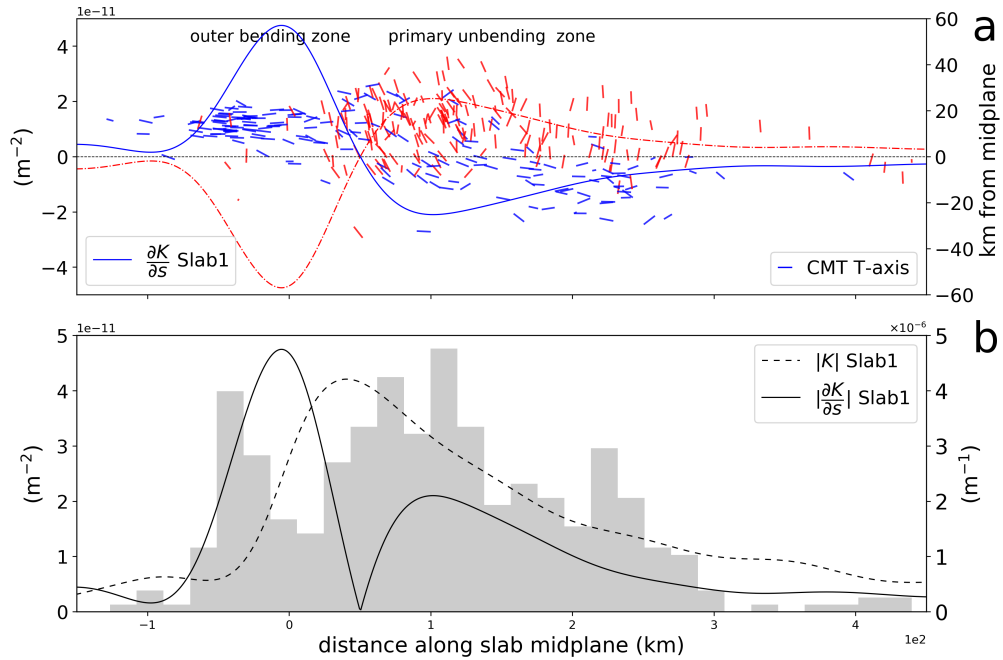
Corresponding seismicity geometry relationships for the ePac slabs are shown in Figs. 20, 21, and 22. As we noted in Section 4, there are far fewer OBZ earthquakes in

Figure 17. Summary of Tonga slab seismicity-geometry relationships. a) CMT T-axes are plotted in a slab midplane coordinate system, with distance from the hypocenter to the midplane shown on the vertical axis, and distance along the midplane relative to the trench (horizontal axes). The T-axes have been rotated so that the angle relative to the midplane is preserved. As in Fig. 6, the T-axes of the CMT moment tensors are plotted as uniform-length vectors, projected along a trench-perpendicular vertical plane. The length variation in the plotted T-axes reflects the magnitude of the projected component of the vector. The blue solid line shows the value of the curvature gradient plotted against the distance along the midplane. The red dashed line shows the reflection of the curvature gradient about the midplane. Together, these lines show parts of the slab that are expected to be stretching (blue half) and shortening (red half), due to the advective component of the bending rate; b) Histogram shows the relative variation in number of slab earthquakes as a function of distance along the midplane (earthquakes deeper than 300 km are excluded). Solid and dashed lines show the absolute value of the midplane curvature and the curvature gradient.

Figure 18. Summary of Japan slab seismicity-geometry relationships. See Fig. 17 caption for details of figure organisation and presentation.

Figure 19. Summary of Kuriles slab seismicity-geometry relationships. See Fig. 17 caption for details of figure organisation and presentation.

672 the ePac regions. The small number that do occur, cluster on the landward side from

673 positive peak in curvature gradient. In Peru these plate bending events occur virtually

674 underneath the trench. Again we note that these do not coincide with peak curvature,

675 but tend to cluster between the peak in curvature gradient and the peak in curvature.

676   In Chile and Peru, the point where the curvature gradient switches sign is also co-

677 incident with the transition between the OBZ cluster (DT earthquake above the mid-

678 plane), and the PUZ (DC earthquakes above the midplane). Figs. 20 and Fig. 21 shows

679 that the PUZ events are clustered where the curvature gradient predicts maximum rates

680 of unbending. Hence, while unbending earthquakes in the ePac slabs occur at shallower

681 depths than the wPac, the distributions are consistent with same basic mechanism. There

682 is no clear evidence of unbending-related earthquakes in central America. Moreover the

683 zone of normal faulting, associated with plate bending, seems to continue in the land-

684 ward direction, past the point when the curvature gradient changes sign. These patterns

685 are difficult to interpret, and clearly do not fit with the systematic variation between plate

686 bending - slab unbending, that we see in the other regions.

687   Whereas the wPac slabs unbend monotonically, the ePac slabs all exhibit additional

688 zones of positive (and negative) curvature gradients. In Chile, a zone of positive curva-

689 ture gradient begins at about 200 km downdip from the trench (Fig. 20) corresponding

690 to the zone where the partially flattened slab begins to increase in curvature, and there-

691 after dip more steeply toward the transition zone. Because of the curvature increase, the

692 upper half of the slab is predicted to be undergoing extension. This zone has a strong

693 spatial overlap with the belt of DT seismicity along the Chile slab at ~ 100 km depth,

694 the most active part being the north Chile seismic belt (see Fig. 9). The full downdip

695 seismic expression Chile, shows a remarkable set of transitions, where earthquakes in the

696 upper half of the slab change from DT (OBZ) to DC (PUZ) and then back to DT where

697 the slab is partially flattened, each transition correlating with the changing sign of the

698 curvature gradient. Low seismic activity prevails in the intervening regions where bend-

699 ing rates are predicted to be negligible. This is very much analogous to the deformation

700 pattern exhibited in the numerical model.

701   Two potential inconsistencies arise in trying to connect the intermediate depth earth-

702 quake belt in Chile with bending. The first is that in the CMT catalog, there is no in-

703 dication of a lower plane of DC seismicity (although Comte et al. (1999) showed they

704 may be present in micro-seismicity). Nevertheless, as we summarise in the Discussion,

705 such asymmetry seems to be the normal expression in zones where slab curvatures is in-

706 creasing. The second problem is that, as we see in Fig. 12 and Fig. 20, a smaller num-

707 ber of DT events seem to lie well below the inferred midplane, a pattern that would seem

708 to be more consistent with uniaxial stretching of the slab. We need to recall, however,

709 that some variability in the lateral morphology of the slab occurs, due to the significant

710 distance across which we aggregate the seismicity (as discussed in Section 2). Moreover,

711 this variability tends to increases with depth (or at least distance from the trench). In

712 Fig. B.2 we show a cross section for a much narrower lateral extent within the north Chile

713 seismic belt (see figure caption for details). In this smaller region, the hypocenter loca-

714 tions are predominately located in the upper $\sim$ 10-20 km of the slab, consistent with seis-

715 micity being localised above the neutral plane. However, we note that some deeper events

716 - potentially outliers - still remain.

717   In Peru, earthquakes in the PUZ transition to sparse DT seismicity in the flat slab.

718 The intensity of this DT seismicity increases towards the distal hinge of the flat slab. Fig

719 21 shows that curvature gradients are generally positive, although small, within the Peru

720 flat slab. They increase rapidly towards the distal hinge of the flat slab, consistent with

721 the increase in seismicity. As in Chile, the bending associated with these positive cur-

722 vature gradients will create extension above the slab midplane. Hence, it plausible that

723 the DT seismicity is the expression of upper plane events in a bending slab. If DT earth-

724 quakes in Peru are related the upper-plane of bending zones, it means that, like Chile,

725 shortening below the neutral plane must be entirely aseismic. The idea that these DT

726 earthquakes are upper-plane conflicts with the impression that, many of the Peru flat

727 slab DT events appear to be beneath the inferred midplane (based on the region aver-

728 aged Slab2 model). Again, we think it is plausible that is artifact due to unconstrained

729 variations in the slab morphology.

730   In Fig. 21 we see a group of slightly deeper earthquakes cluster at the far landward

731 edge of the domain ($>$ 650 km along the slab midplane), located beyond the zone of pos-

732 itive curvature gradient. These have been highlighted using a greater transparency level,

733 and are excluded from the histogram in the lower panel of Fig. 21. These are mainly events

734 in the Pucallpa seismic nest (see Fig. 10 upper panel). It is reasonable to assume these

735 are associated with a localised geometric discontinuity in the slab, which is unrelated to

736 the advective bending signal we are trying to resolve (Gutscher et al., 2000; Wagner &
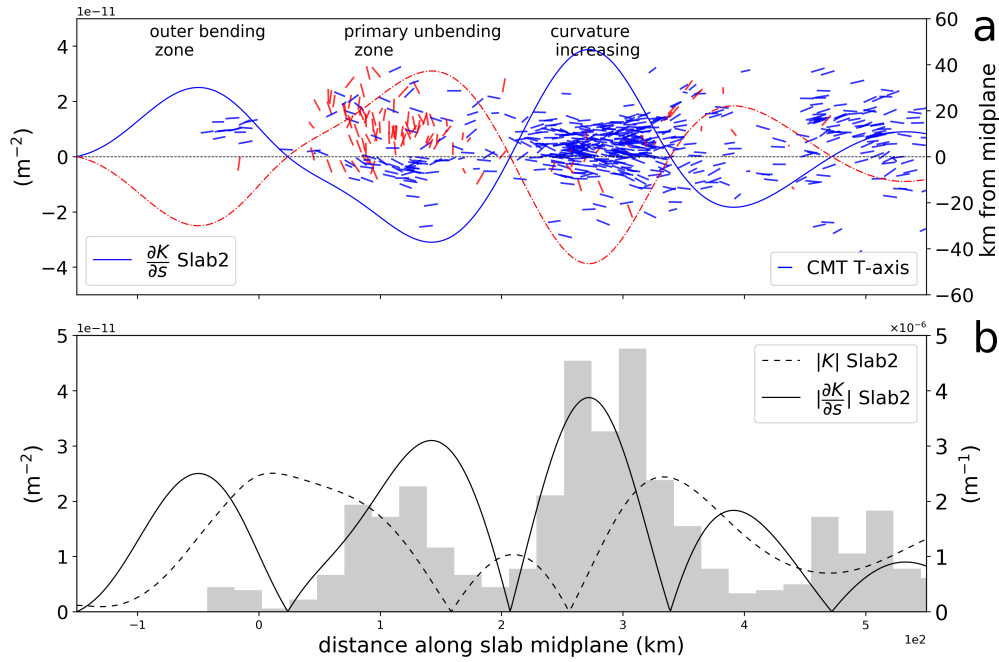
Figure 20. Summary of Chilean slab seismicity-geometry relationships. See Fig. 17 caption for details of figure organisation and presentation.

Okal, 2019). Recall that the advective bending signal we explore, inferred through curvature gradient, contains no information about lateral geometric variations, or time-dependent modes of deformation (i.e. changes in slab geometry that are occurring in an upper plate reference frame).

7 Discussion

7.1 Ubiquity of bending/unbending

In reference to northern Japan, Kawakatsu (1986a) argued that peak rates of geometric unbending (i.e. the advective bending rate) were likely to be higher than uniform stretching due to slab pull. Yet it is only in a few regions, northern Japan, Kuriles and Aleutians, where unbending has been recognised as a dominant control on slab seismicity. In particular, the role of unbending has very seldom been discussed in the context of ePac slabs (Isacks and Barazangi (1977) is one study we are aware of). In this study we have shown that earthquakes consiitent with unbending are present in both wPac and ePac margin slabs. The region of Central America considered here is an exception, with no clear DC earthquakes. We note, however, that along other sections of the Mid-
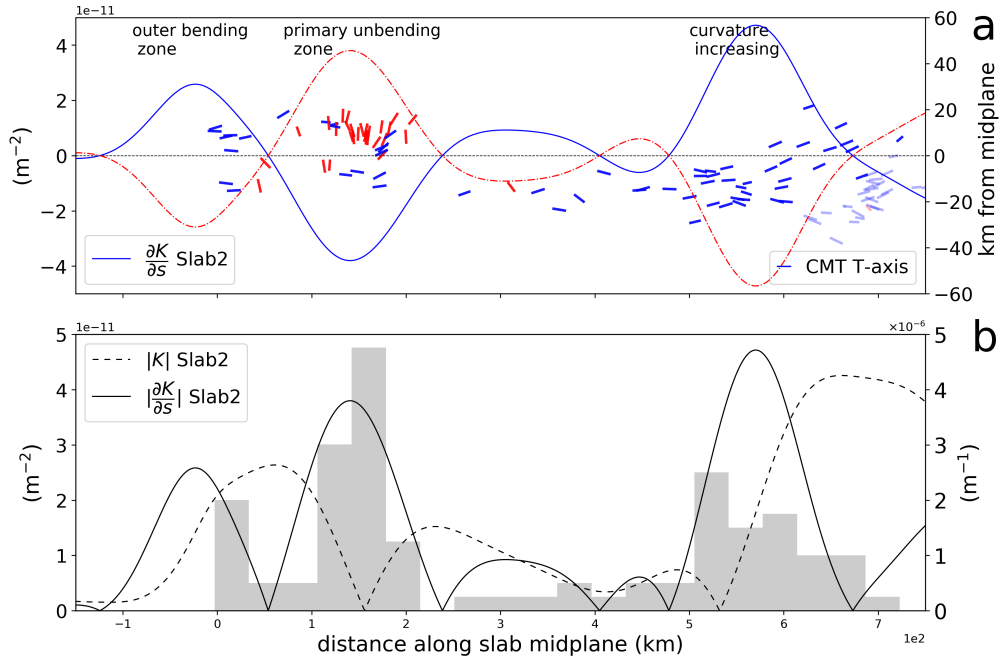
Figure 21. Summary of Peruvian slab seismicity-geometry relationships. See Fig. 17 caption for details of figure organisation and presentation.
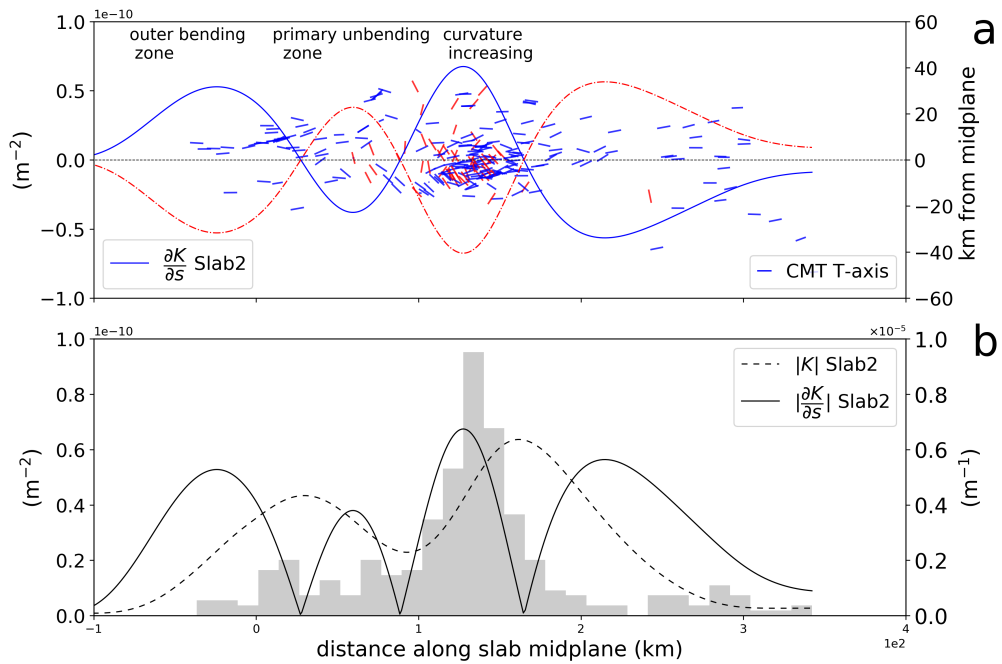
Figure 22. Summary of Central American slab seismicity-geometry relationships. See Fig. 17 caption for details of figure organisation and presentation.

752 dle America Trench, DC earthquakes characteristic of unbending are present (i.e. in the

753 Mexican Flat slab region, see D. Sandiford, Moresi, Sandiford, and Yang (2019)). In most

754 cases the PUZ is expressed as a polarised DSZ, with DC earthquakes occurring above

755 (in a slab normal sense) a deeper band dominated by DT mechanisms. These polarised

756 DSZs are consistent with the seismic expression of stretching/shortening either side of

757 the neutral plane. However, the relative number of DT earthquakes compared to DC is

758 quite variable, as exemplified in the difference between Tonga and Kuriles (c.f. Fig. 6

759 and 8). We discuss this variability in the following sections.

760 The depth where PUZ earthquakes cluster varies substantially, with the ePac zones

761 being consistently shallower depths than wPac. These variations are consistent with sys-

762 tematic variations in slab geometry, whereby ePac slabs unbend at correspondingly shal-

763 lower depths. The fact that ePac PUZs are shallower than the normal intermediate depth

764 specification (> 70 km), may be one reason they have been somewhat neglected. In any

765 case, the close proximity of ePac PUZ events to the megathrust means that filtering the

766 signal from the latter is critical. Resolving the ePac PUZ requires aggregated along large

767 lateral distances, at least when considering events within the magnitude range of the CMT

768 catalog.

769 The occurrence of isolated DC earthquakes in the unbending zone of the Chile slab

770 was noted by Lemoine et al. (2002), who proposed the term 'slab push earthquakes' to

771 describe them, so as to distinguished them from more typical 'slab pull' (i.e. DT) earth-

772 quakes. While Lemoine et al. (2002) mention a possible relationship between the DC events

773 and slab unbending, they do not interpret the entire set of shallow intraslab earthquakes

774 (both DC and DT) as a DSZ associated with unbending. Isacks and Barazangi (1977)

775 suggest that DC earthquakes in Peru are related to unbending, an interpretation that

776 our study supports. Fuenzalida, Schurr, Lancieri, Sobiesiak, and Madariaga (2013) pro-

777 vide high-resolution aftershock solutions following a medium size DC event in the un-

778 bending zone of the Chile slab (Mw 6.1 Michilla Earthquake, Dec. 16, 2007). The af-

779 tershock sequence delineates a near-vertical fault plane between about 40 and 50 km depth.

780 This orientation is consistent with reactivation of a steep landward-dipping outer-rise

781 normal fault plane, and provides an important insight into the rupture character of a shal-

782 low DC unbending event. The identification of a compelling unbending signal in the Nazca

783 plate in Chile and Peru is important in the context of thinking about the overall dynamic

784 state of the slab. Following (Kawakatsu, 1986a) it means that in the PUZ, rates of short-

785 ening above the neutral plane must exceed the 'background' rate of uniform stretching.

786 This does not rule out, of course, that stretching rates may be non-uniform, and could

787 for instance become larger at depths beyond the PUZ (e.g. Bloch et al., 2018). Overall,

788 our results strongly support Kawakatsu's argument about the relative magnitudes of ge-

789 ometric unbending versus uniform stretching.

7.2 Geometric bending and contrasting seismic expression

791 The role of geometric bending has mainly been explored in relation to wPac slabs,

792 where the process of unbending (PUZ) occurs over a larger downdip distance and peaks

793 at greater depth than ePac. In the wPac slab regions we have considered, inferred rates

794 of unbending decay monotonically as slabs straighten out in the mid-upper mantle, con-

795 sistent with the gradual falloff in seismicity. These wPac-type slab morphologies are of-

796 ten presented as the archetypal subduction geometry. However, subduction along much

797 of the ePac margin is characterised by alternating fully and partially flattened slab sec-

798 tions. While constraining the precise geometry of ePac slabs remains a challenge, the gen-

799 eral picture of these more complex morphologies is fairly well established (Engdahl et

800 al., 1998; Hayes et al., 2018; Isacks & Barazangi, 1977). We argue that these systematic

801 geometric differences are the key control on the contrasting seismic expression of ePac

802 and wPac slabs at intermediate depths. Analysis of the downdip curvature gradient shows

803 that the Nazca plate fully unbends at depths of around 60 km. Beyond this, additional

804 zones of bending occur, which are associated with full or partial slab flattening. The ma-

805 jority of ePac DT seismicity is conspicuously clustered in curvature-increasing zones. We

806 summarise these systematic geometric differences between wPac and ePac in Fig. 23.

807 If advective bending is the dominant control for localising DT seismicity in ePac

808 slabs, it requires that the lower half of the bending regions (i.e. beneath the neutral plane)

809 is almost completely aseismic. In this light an important observation is that an oppo-

810 sitely polarised DSZ has been observed in microseismicity, near the northern limit of our

811 Chile study region (18°S) (Comte & Suarez, 1994).

812 Micro-seismicity aside, the lack of significant lower plane events in these putative

813 bending zones, like the north Chile seismic belt, may seem at odds with the presence of

814 lower plane events updip in the PUZ. However, this actually follows a pattern that is quite

815 consistent, throughout different depths, in most subduction settings we analyse. Specif-

ically, it appears that the seismic expression of zones of increasing curvature tends to more asymmetric (less lower plane activity) than the expression of decreasing curvature. For instance, the OBZ is normally dominated by upper plane DT events, whereas in the PUZ, we tend to see lower plane events more strongly. A simple explanation for this is that the flexural stress state is modified by a uniaxial component, due to slab pull, acting in a sense of effective tension. This is expected to modify the relative depth of the neutral plane of bending (e.g. Craig et al., 2014). In zones of increasing curvature, the flexural stress state in the upper half of the slab is tensional (see next Section for discussion of relationship between stress and strain rates). Relative to pure bending, a uniaxial tensional component would be expected to shift the neutral plane deeper, closer to, or even beyond the brittle ductile transition, at around 600 - 700 °C. In zones of decreasing curvature, the opposite applies, with the neutral plane shifting towards the slab surface into colder parts of the slab, enhancing the prospect of seismic strain occurring beneath the neutral plane. This describes a systematic pattern we see in the Kuriles, Japan, Chile and Peru. Hence, the absence of lower plane events in the north Chile seismic belt, or the Peru flat slab, is compatible with a similar absence in the OBZ of the Kuriles and Japan.

In this context Tonga is anomalous in that the pattern is systematically reversed compared to the other slabs. In Tonga, we observe a more symmetric pattern, characterised by numerous lower plane earthquakes in the OBZ, amd a less symmetric pattern with far fewer lower plane earthquakes in the PUZ. The could indicate that, relative to other settings, the magnitude of the uniaxial stress component due to slab pull is reduced (or possible even reversed). This concurs with earlier ideas that the seismic expression in Tonga has a more compressive signal than other slab regions (Gurnis et al., 2000; Isacks & Molnar, 1971; Nothard, McKenzie, Haines, & Jackson, 1996). Alternatively, a significant change in slab strength profile may also alter the depth of the neutral plane (e.g Craig et al., 2014). However, the systematic reversal of the DSZ symmetry patterns, with respect the the other slabs, is most easily explained through the affect of a uniaxial stress component.

7.3 Slab rheology, strain rates and elasticity

It is well understood that deformation of the lithosphere is accommodated by elastic as well as a range of inelastic mechanisms. Investigations focused on the loading of
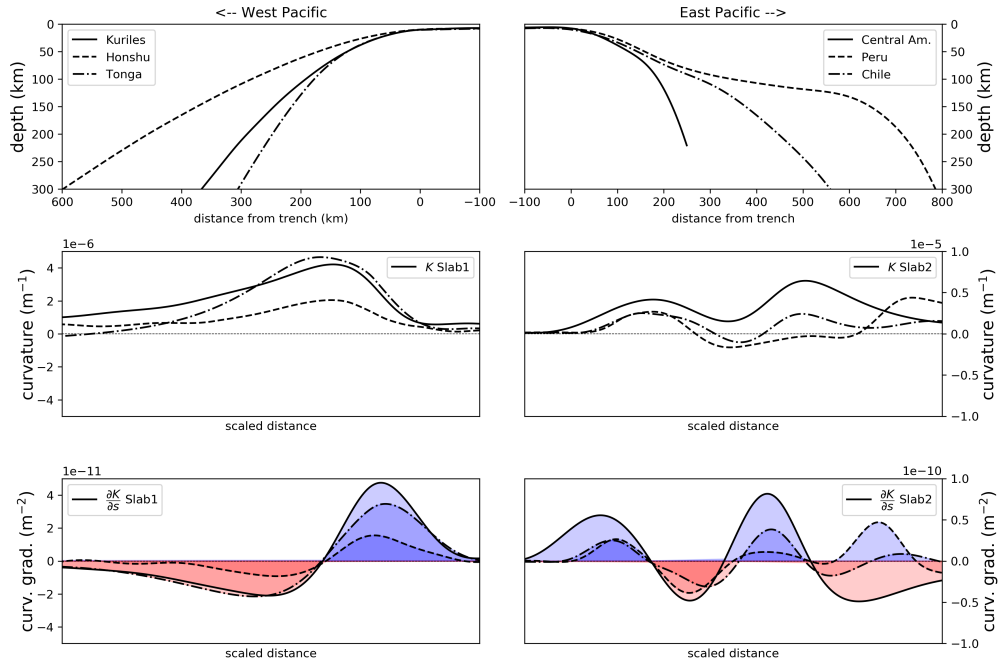
Figure 23. Comparison of characteristic features of wPac (left) and ePac (right) slab geometries. Upper panel shows slab profiles, middle panel shows curvatures and lower panels show curvature gradients. The advective rate of bending is governed by the curvature gradient. In the lower two panels (either side) we have scaled the horizontal distance (distance along the midplane) so that the transition from the OBZ to the PUZ lies at the same point (i.e. the first zero crossing of the curvature gradient is equal for the ePac and wPac groups respectively).

oceanic lithosphere, including the bathymetry profile of plates near the trench, has tended to emphasise the elastic nature of plates. On the other hand, the existence of earthquakes, along with a range of other inferences, suggests that inelastic deformation must account for much of the total strain accumulation during bending in the subduction hinge (Billen, 2005; Chapple & Forsyth, 1979; Engdahl & Scholz, 1977; Sleep, 1979).

Turcotte, McAdoo, and Caldwell (1978) argued that the Kuriles bathymetry was consistent with the bending of a constant thickness elastic plate, while the more strongly curved Tonga profile implied a significant region of plastic failure in the plate. McAdoo, Caldwell, and Turcotte (1978) argued that the Kuriles bathymetry was better fit by an elasto-plastic rheology. These conflicting findings reflect differing assumptions, such as the magnitude of the in-plane compressive force, which is finite in the McAddoo model, as well as the initial elastic thickness of the undeformed lithosphere. Recent global analyses have argued that weakening of the plate, with an associated reduction in the elastic thickness at the outer rise, uniformly improves the fit of predicted profiles to observed bathymetry and gravity (Hunter & Watts, 2016). Hence, while early studies seemed to show that plates, at least in some cases, exhibited a purely-elastic response in the vicinity of the trench, ongoing work casts doubt on this result.

At peak curvature the potential elastic stress in slabs is of the order of 10 GPa (e.g. D. Sandiford et al., 2019). Because this is at least an order of magnitude larger than inferred slab yield stresses (Chapple & Forsyth, 1979), inelastic yielding would be expected to accommodate the large proportion of bending strains in slabs (Engdahl & Scholz, 1977; Wang, 2002). As previous studies have noted, a primary mechanism for plastic strain at yield is the slip accompanying earthquakes (Chapple & Forsyth, 1979; Sleep, 2012). An important consequence of inelastic deformation is the fact that the flexural stress state is often inverted with respect to the sign of the slab curvature. Indeed the premise that earthquakes occur as a response to slab unbending (where the curvature is still positive) reflects the assumption of significant inelastic deformation. We argue that in the limit of very weak slabs, where the majority of strain is accommodated by inelastic deformation, the flexural stress state will tend to approximate the bending rate, not the curvature. When the sign of the bending rate changes, the flexural stress will rapidly (compared to the change in the sign of the curvature) evolve to match the sign (polarity) of the bending rate. In this study we have emphasised that, to first order, the orientation of seismic moment tensors correlates with the inferred bending rate (i.e. curvature gra-

881 dient), rather than total strain (i.e. curvature). This relationship supports previous work

882 suggesting that slabs must yield rapidly after the onset of bending in the hinge (Billen,

883 2005; Engdahl & Scholz, 1977; Sleep, 2012).

7.4 Implications for subduction dynamics

885 The sources of buoyancy that drive pate motions are often separated into density

886 anomalies in the surface plates (e.g. ridges and other topography) and sublithospheric

887 sources (e.g. slabs) (e.g Coblentz, Richardson, & Sandiford, 1994; Ghosh, Holt, & Flesch,

888 2009). How much of the slab density deficit is propagated through the slab into the sur-

889 face plates has been an ongoing debate in geodynamics. Attempts to understand the global

890 distribution of plate velocities, for instance, have concluded that a large fraction of slab

891 weight must be propagated through the slab (Conrad & Lithgow-Bertelloni, 2002; Forsyth

892 & Uyeda, 1975; van Summeren, Conrad, & Lithgow-Bertelloni, 2012). While the pres-

893 ence of intermediate depth DT zones does not constrain the magnitude of stress in slabs,

894 the inference of uniform stretching in slabs is clearly compatible with the idea that stresses

895 due to slab pull are significant (e.g. Molnar & Bendick, 2019). With simple assumptions

896 made about effective slab rheology, stresses in the order of 100s of MPa, have previously

897 been estimated (Conrad & Lithgow-Bertelloni, 2004). While the notion that slabs un-

898 dergo uniform stretching seems consistent with inferences about the forces driving plate

899 motion, the paradox remains as to why the seismic expression of 'slab pull' is evidently

900 not expressed in wPac slabs, which are attached to the fastest moving large plate. One

901 suggestion is that these DC slabs subduct at rates faster than their terminal (Stokes)

902 sinking velocity, and hence undergo uniform shortening (Forsyth & Uyeda, 1975; Fujita

903 & Kanamori, 1981b).

904 Other lines of evidence suggest slab pull must be significantly smaller than inferred

905 from plate velocity considerations. Coblentz et al. (1994) argued that the intraplate stress

906 field is largely explicable in terms of a balance between lithospheric potential-energy dis-

907 tribution and plate-boundary resistance, implying a relatively low degree of slab-plate

908 coupling in plates is the norm. These results are implicit in other modelling studies, which

909 capture the first order features of the intraplate stress field without considering any sub-

910 lithospheric sources (e.g. Ghosh et al. (2009)). Based on stress indicators in the central

911 Indian Ocean M. Sandiford, Coblentz, and Schellart (2005) showed that the effective slab

912 pull fraction must be low, around 0.1 in order to account for large magnitude reverse fault

913 mechanisms observed in the central Indian Ocean with P-axes parallel to the Sumatran

914 trench, implying a average deviatoric tensional stress no more than order 10 MPa prop-

915 agated via the slab.

916 The dominant control of bending over stretching in slab seismic strain release is

917 a characteristic of slabs in the Stokes regime, where resistance to slab weight is primar-

918 ily supplied by drag from the mantle (F. A. Capitanio et al., 2009; Goes, Capitanio, Morra,

919 Seton, & Giardini, 2011). In this study we highlight that slabs in the Stokes regime can

920 develop highly-diverse internal deformation patterns. The diversity in strain patterns

921 in slabs arises from the curvature-gradient dependence of the advective bending rate. We

922 show that the pervasive DT expression of slab in the ePac appears to be linked to zones

923 of curvature increase at intermediate depths. Relatively subtle changes in slab morphol-

924 ogy, such as the partial flattening of the slab in northern Chile, create alternating zones

925 of bending and unbending over relatively short wavelengths. A feature of our framework

926 is that it obviates special appeals to fundamental differences in slab stress (or strength)

927 between different slabs, such as is required in the conventional interpretation of uniform

928 stretching in Chile, and shortening in Tonga (e.g. Fujita & Kanamori, 1981b; Isacks &

929 Molnar, 1971).

930 In the framework we propose, contrasts in ePac and wPac seismic expression arise

931 due to systematic differences in slab morphology. In the ePac, zones of positive bend-

932 ing rate are associated with full or partial slab flattening. Recent work suggest that these

933 slab-morphology contrasts may be controlled by kinematics of the upper plates with re-

934 spect to large-scale mantle flow (Yang et al., 2019). Atlantic Ocean opening allows fast

935 trench-ward motion of South America, which promotes compression-dominated tecton-

936 ics in the overriding plate, that has been argued to provide the pre-conditions for flat-

937 slab development along the ePac margin (Manea & Gurnis, 2007; W. Schellart, 2017; van

938 Hunen, van den Berg, & Vlaar, 2004; Yang et al., 2019). In contrast, large-scale down-

939 welling beneath Asia, revealed by seismic imaging, geodynamic models, and plate recon-

940 structions seems to restrain trench-ward motion of East Asia. Along with the greater

941 ages of wPac slabs, this promotes steeper subduction, and extension-dominated upper-

942 plate tectonics (Yang et al., 2019).

943 Our framework also provides an interesting perspective on the dynamics of intra-

944 continental intermediate depth seismic zones such as Hindu Kush and the Vrancea zone

beneath the Carpathians, where seismic strain rates exceed $10^{-14}s^{-1}$ (Lorinczi & House-
man, 2009; Molnar & Bendick, 2019). These are an order of magnitude greater than typ-
ical intermediate depth seismic strain in subducting slabs ($\sim 10^{-15}s^{-1}$). The strain rates
beneath the Hindu Kush and Vrancea are consistent with a regime of uniform stretch-
ing associated with lithospheric necking (Lister, Kennett, Richards, & Forster, 2008; Lor-
inczi & Houseman, 2009). It is precisely because DT slabs (e.g. Chile) are not necking
that seismic strain rates are much lower. They are, instead, controlled by rates of ge-
ometric bending, which reconciles the observed seismic release rates closer to $10^{-15}s^{-1}$)
(Kawakatsu, 1986a).

7.5 Limitations and future work

In trying to establish the basic spatial correlation between bending rates and slab
seismicity, we have focused on the advective component of the bending rate (Buffett, 2006;
Ribe, 2001, 2010). The time-independence allows us to infer the relative variation in long-
term bending rates from present day slab geometry. The advective component of the bend-
ing rate should be the dominant bending term for slabs in which: a) the hinge morphol-
ogy is not changing rapidly, and b) three-dimensional (along-strike) contributions to the
stress/deformation are relatively minor (Buffett & Becker, 2012; Buffett & Heuret, 2011).
Clearly these conditions may not be met in all slab regions, and this caveat will require
careful attention in trying to test this hypothesis in other settings. In this study we have
primarily focused on the variation in the orientation of seismicity (moment tensors) with
respect to slab geometry (curvature gradient). We have been more circumspect about
the correlation between seismicity rates and the relative magnitude of the curvature gra-
dient. This is primarily because seismic activity rates are not necessarily proportional
to the long term strain rate (i.e. the bending rates inferred via the curvature gradient).
The influence of metamorphism and fluids is one effect which is likely to effect the rates
of seismicity. It was shown, for instance, that the intermediate depth seismic activity rate
varies with the inferred amount of plate hydration in the outer-rise region (Boneh et al.,
2019), with similar mechanisms being linked to rapid changes seismic expression along-
strike (Shillington et al., 2015). This process is a potential control on dramatic changes
in seismic activity rates between the north Chile seismic belt, and parts of the Nazca slab
further south (e.g. Fig. 9). Another factor to consider is simply the increasing role of
ductile deformation as the slab heats up from above and below. As a result, the relative

amount of seismic/ductile deformation is likely to vary in a complex manner with changes in pressure and temperature. Finally, short catalog times are likely to also bias the relative number of earthquakes in different parts of the slab. We highlight, for instance, the increase in OBZ seismicity in Northern Japan following the Tohoku earthquake. The number of earthquakes is likely to include a range of transient signals.

In the regions we have addressed, there are number of instances where the correlation between curvature gradient and seismic expression is ambiguous, absent, or opposite to what we would expect. We briefly discuss a few of examples, some of which we think are readily explained, and some not. In the ePAc settings, we have discussed clusters of seismicity which are likely to be unrelated to the advective bending mode. The Pucallpa seismic nest in Chile is an example of a seismicity cluster that apparently correlates with a relatively localised trench-parallel perturbation of the slab morphology (Gutscher et al., 2000; Wagner & Okal, 2019). This is region where deformation of slab is likely to involve lateral, time-dependent changes in slab morphology.

In the case of Chile, we demonstrate a close spatial association between the main peak in positive curvature gradient (see Fig. 20) and the primary cluster of DT seismicity (the north Chile seimsic belt, see Fig. 9). However, the relationship becomes increasingly inconsistent at greater depths. Based on our geometric analysis, the slab would be expected to go through an additional zone of unbending (i.e. a secondary unbending zone), where the sign of the curvature gradient returns to negative (e.g. Fig. 20). This transition is also seen in the numerical model, which predicts a return to downdip shoring at around 550 km from the trench (which is seen in the far RHS in the lower panel of Fig. 16). And yet we see no persuasive evidence that DC earthquakes (e.g. upper plane unbending earthquakes) occur at this depth in Chile, or for that matter in Peru or Central America. These predicted secondary unbending zones are missing, and this remains difficult to explain in our framework, unless we appeal to increasing magnitude of slab stretching rates, relative to advective bending rates, at these depths (Bloch et al., 2018), or that the upper-part of slab has become by this stage aseismic (potentially through warming and/or dehydration).

8 Conclusions

Our study suggests that the 'fingerprints' of flexure in slab seismicity are more significant than previously realised. We have analysed the contribution of the advective bending rate, and found that in several key locations, the orientation of slab seismic moment tensors vary systematically with the anticipated sense of defomation. The fact that flexure controls seismicity patterns in the plate bending domain (OBZ) is of course, already widely accepted, as is the effect of unbending in a limited number of slab settings. In terms of extending the role of bending/unbending, our contributions are twofold. Firstly we show that seismicity characteristic of unbending is prevalent in ePac slabs, albeit at shallower depths than wPac slabs. We then show that geometric differences between ePac and wPac slabs lead to additional zones of bending at intermediate depths in ePac slabs. The majority of ePac DT seismicity is conspicuously clustered in these curvature-increasing zones, which are associated with full or partial slab flattening. Hence, the contrasting seismic expression in ePac and wPac slabs appears to arise due to systematic differences in slab morphology - rather than through significant differences in subduction force balance, as implied in previous conceptual frameworks. We argue that the observed correlation of seismic of earthquake orientation with the curvature gradient (and not curvature) arises from the fact that a very significant proportion of bending strain is accommodated by inelastic deformation, of which seismic slip itself is a key component.

A Numerical model setup

The model was developed using the Underworld2 code, and follows closely the setup described in (D. Sandiford & Moresi, 2019), to which we refer readers for a description of the governing equations, numerical method, mantle rheology, and implementation of the subduction interface. Compared to (D. Sandiford & Moresi, 2019), we have made two noteworthy changes in the setup of model discussed here: 1) We use a larger domain, with a higher relative resolution; 2) we constrain the upper viscosity limit in a small part of the mantle wedge to a value of 1. The geometry of the viscosity-limited section of the wedge is shown in Fig. A.1. This element of the model constitutes a very simplified attempt to account for processes such as the presence volatiles and melts in the wedge. These are expected to substantially reduce the effective viscosity, compared to the dry melt-free conditions that are reflcted in our model creep law (diffusion creep). In terms of the model evolution the viscosity limit applied to this region has the primary effect of allowing asymmetric subduction to proceed even when the slab dip angle becomes quite shallow, and the upper plate has thickened (both due to cooling and a degree of shortening). If we did not provide this upper limit on the viscosity, the shallow part of mantle wedge would increase in viscosity as the slab dip decreases, due to reduction in temperature. This creates increased coupling with upper plate, and a rapid feedback cycle that results in a breakdown of single-sided subduction.

Fig. A.1 provides an overview of the model domain, as well as initial and boundary conditions. The depth of the domain is 1500 km, and the aspect ratio is 6. Initial temperature conditions define two plates which meet at the centre of the domain, including a small asymmetric slab following a circular arc to a depth of 150 km. The subducting plate has an initial age of 50 Myr at the trench, while the upper plate age is 10 Myr. Both plates have a linear age profile with an initial age of zero at the sidewalls. This setup allows the model to evolve under the driving force of internal density anomalies which is therefore regarded as a fully dynamic model. Apart from the presence of a WL, there is no compositional difference between the subducting and upper plate, nor do we include any compositional differentiation within the oceanic lithosphere. The only aspects of the model setup that are varied are the details of subduction interface implementation (described in the following section) and the model resolution.

Approximate solutions to the incompressible momentum and energy conservation equations are derived using the finite element code Underworld2. Underworld2 is a Python API which provides functionality for the modelling of geodynamic processes. Underworld2 solves the discrete Stokes system through the standard mixed Galerkin finite element formulation. The domain is partitioned into quadrilateral elements, with linear elements for velocity and constant elements for pressure. Material properties are advected on Lagrangian tracer particles.

The model has a mesh resolution of 392 elements in the vertical direction, refined to provide an element width of ~ 1 km near the surface, and a particle density of 30 tracers per element. Particles are added and removed to maintain density near this value. During quadrature, material properties are mapped to quadrature points using nearest-neighbour interpolation. The Lagrangian tracer particles are used to distinguish the subduction interface material from the rest of the system (lithosphere and mantle). Underworld2 solves the energy conservation equation using an explicit Streamline Upwind Petrov Galerkin (SUPG) method. In this approach, a Petrov-Galerkin formulation is obtained by using a modified weighting function which affects upwinding-type behaviour. The Stokes system has free-slip conditions on all boundaries. The energy equation has constant (Dirichlet) and zero-flux (Neumann), on the top and bottom boundary respectively. The left and right sidewalls have a constant temperature equal to the mantle potential temperature (1673°K). The surface temperature is 273°K.
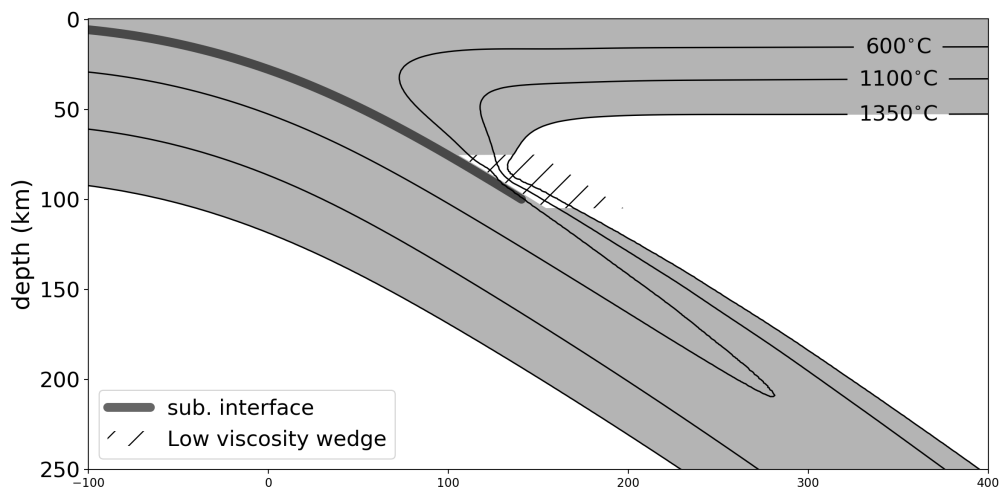
Figure A.1. Detail of numerical model at 10 Myr. The grey region shows parts of the model colder than 1350°C (model potential temperature is 1400 °C). The hatched region shows the part of the mantle wedge in which the upper limit of viscosity is set to 2×10^{20} Pa s.

Parameter name	Value	Symbol	Units
domain depth	1000	-	km
domain width	5000	-	km
potential temp	1673	T_p	K
surface temp	273	T_s	K
viscosity min.	1×10^{18}	-	Pa s
viscosity max.	1×10^{24}	-	Pa s
diffusion creep volume UM**	5.27×10^{-6}	V	$m^3\,mol^{-1}$
diffusion creep energy UM	316	E	$kJ\,mol^{-1}$
diffusion creep constant UM	1.87×10^9	A	$Pa^n\,s^1$
diffusion creep volume LM***	1.58×10^{-6}	V	$m^3\,mol^{-1}$
diffusion creep energy LM	210	E	$kJ\,mol^{-1}$
diffusion creep constant LM	1.77×10^{14}	A	$Pa^n\,s^1$
DP* friction coefficient	0.1	μ	-
DP cohesion	20	C	MPa
yield stress max.	200	τ_{max}	MPa
sub. interface thickness	10	W_{init}	km
sub. interface max. thickness	19	W_{max}	km
sub. interface min. thickness	10	W_{min}	km
sub. interface viscosity	5×10^{19}	-	Pa s
sub. interface depth taper start	100	-	km
sub. interface depth taper width	30	-	km
LVW† viscosity	2×10^{20}	-	Pa s
LVW upper depth	45	-	km
LVW lower depth	150	-	km
slab age at trench	50	-	Myr
slab radius of curv.	200	-	km
initial slab depth	150	-	km
upper plate age at trench	10	-	Myr
lower mantle viscosity increase	15	-	-
adiabatic temp. gradient	3.7×10^{-4}	-	-
internal heating	0.0	Q	W.m^{-3}

Table A.1.   Dimensional model parameters. * Drucker-Prager, ** Upper Mantle, *** Lower mantle. ‡: Low Viscosity Wedge. Typical model element resolution was 800 × 160.
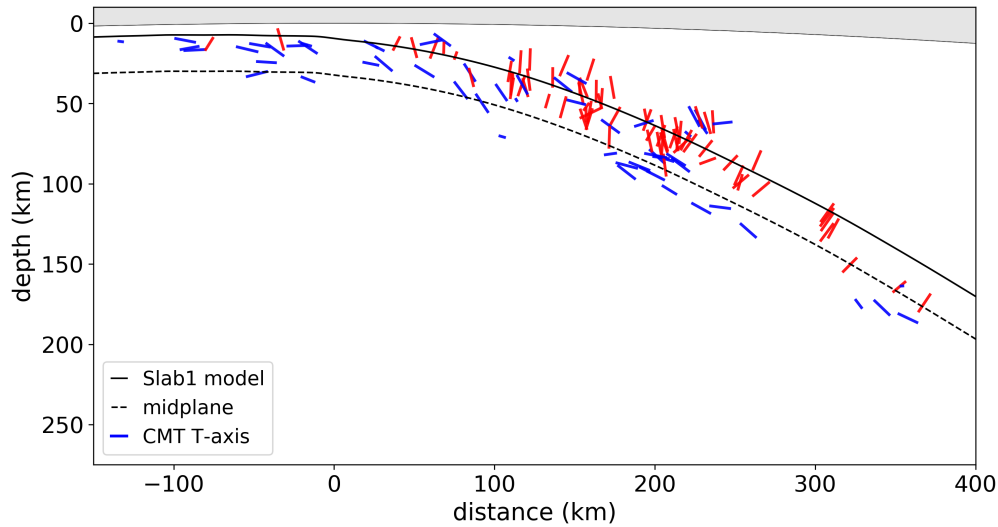
Figure B.1. Cross section of CMT T-Axes for Japan region (northern Honshu), for period before Tohuku earthquake (11/03/2011)

B Additional Figures

Acknowledgments

References

Amante, C., & Eakins, B. W. (2009). Etopo1 arc-minute global relief model: procedures, data sources and analysis.

Bailey, I. W., Becker, T. W., & Ben-Zion, Y. (2009, June). Patterns of co-seismic strain computed from southern california focal mechanisms. *Geophysical Jour-*
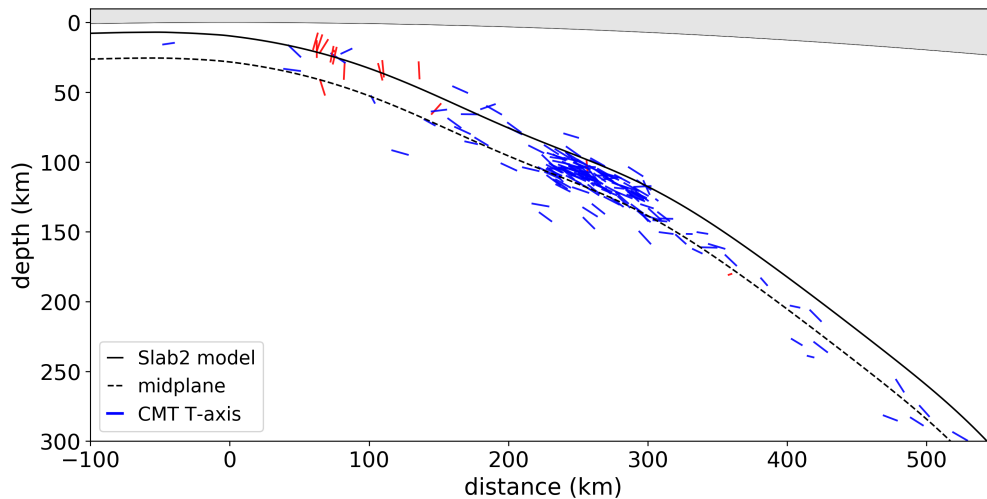
Figure B.2. Chile cross section for restricted domain, normal to the South American trench between 18.5° and 22° south. This region is also represented by the transparent green band in Fig. 9.

nal International, *177*(3), 1015–1036. Retrieved from https://doi.org/10.1111/j.1365-246x.2009.04090.x doi: 10.1111/j.1365-246x.2009.04090.x

Barazangi, M., & Isacks, B. (1976). Spatial distribution of earthquakes and subduction of the nazca plate beneath south america. *Geology*, *4*(11), 686. Retrieved from https://doi.org/10.1130/0091-7613(1976)4<686:sdoeas>2.0.co;2 doi: 10.1130/0091-7613(1976)4⟨686:sdoeas⟩2.0.co;2

Billen, M. I. (2005). Constraints on subducting plate strength within the Kermadec trench. *Journal of Geophysical Research*, *110*(B5). Retrieved from http://dx.doi.org/10.1029/2004jb003308 doi: 10.1029/2004jb003308

Billen, M. I., Gurnis, M., & Simons, M. (2003, May). Multiscale dynamics of the tonga-kermadec subduction zone. *Geophysical Journal International*, *153*(2), 359–388. Retrieved from https://doi.org/10.1046/j.1365-246x.2003.01915.x doi: 10.1046/j.1365-246x.2003.01915.x

Bloch, W., Schurr, B., Kummerow, J., Salazar, P., & Shapiro, S. A. (2018). From slab coupling to slab pull: Stress segmentation in the subducting nazca plate. *Geophysical Research Letters*, *45*(11), 5407–5416.

Boneh, Y., Schottenfels, E., Kwong, K., Zelst, I., Tong, X., Eimer, M., ... Zhan, Z. (2019, April). Intermediate-depth earthquakes controlled by incoming plate

hydration along bending-related faults. *Geophysical Research Letters*, *46*(7),
3688–3697. Retrieved from `https://doi.org/10.1029/2018gl081585` doi:
10.1029/2018gl081585

Brudzinski, M. R., Thurber, C. H., Hacker, B. R., & Engdahl, E. R. (2007, jun).
Global Prevalence of Double Benioff Zones. *Science*, *316*(5830), 1472–
1474. Retrieved from `http://dx.doi.org/10.1126/science.1139204` doi:
10.1126/science.1139204

Buffett, B. A. (2006). Plate force due to bending at subduction zones. *Journal of
Geophysical Research*, *111*(B9). Retrieved from `https://doi.org/10.1029/`
`2006jb004295` doi: 10.1029/2006jb004295

Buffett, B. A., & Becker, T. W. (2012). Bending stress and dissipation in sub-
ducted lithosphere. *Journal of Geophysical Research*, *117*(B5). Retrieved from
`http://dx.doi.org/10.1029/2012jb009205` doi: 10.1029/2012jb009205

Buffett, B. A., & Heuret, A. (2011, jun). Curvature of subducted lithosphere
from earthquake locations in the Wadati-Benioff zone. *Geochemistry Geo-
physics, Geosystems*, *12*(6). Retrieved from `http://dx.doi.org/10.1029/`
`2011gc003570` doi: 10.1029/2011gc003570

Capitanio, F., Morra, G., & Goes, S. (2007, October). Dynamic models of
downgoing plate-buoyancy driven subduction: Subduction motions and en-
ergy dissipation. *Earth and Planetary Science Letters*, *262*(1-2), 284–297.
Retrieved from `https://doi.org/10.1016/j.epsl.2007.07.039` doi:
10.1016/j.epsl.2007.07.039

Capitanio, F. A., Morra, G., & Goes, S. (2009, April). Dynamics of plate bending
at the trench and slab-plate coupling. *Geochemistry, Geophysics, Geosystems*,
10(4), n/a–n/a. Retrieved from `https://doi.org/10.1029/2008gc002348`
doi: 10.1029/2008gc002348

Chapple, W. M., & Forsyth, D. W. (1979, November). Earthquakes and bending
of plates at trenches. *Journal of Geophysical Research: Solid Earth*, *84*(B12),
6729–6749. Retrieved from `https://doi.org/10.1029/jb084ib12p06729` doi:
10.1029/jb084ib12p06729

Chen, M., Manea, V. C., Niu, F., Wei, S. S., & Kiser, E. (2019, February).
Genesis of intermediate-depth and deep intraslab earthquakes beneath
japan constrained by seismic tomography, seismicity, and thermal mod-

eling. *Geophysical Research Letters*, *46*(4), 2025–2036. Retrieved from `https://doi.org/10.1029/2018gl080025` doi: 10.1029/2018gl080025

Coblentz, D. D., Richardson, R. M., & Sandiford, M. (1994, August). On the gravitational potential of the earths lithosphere. *Tectonics*, *13*(4), 929–945. Retrieved from `https://doi.org/10.1029/94tc01033` doi: 10.1029/94tc01033

Comte, D., Dorbath, L., Pardo, M., Monfret, T., Haessler, H., Rivera, L., . . . Meneses, C. (1999, July). A double-layered seismic zone in arica, northern chile. *Geophysical Research Letters*, *26*(13), 1965–1968. Retrieved from `https://doi.org/10.1029/1999gl900447` doi: 10.1029/1999gl900447

Comte, D., & Suarez, G. (1994, January). An inverted double seismic zone in chile: Evidence of phase transformation in the subducted slab. *Science*, *263*(5144), 212–215. Retrieved from `https://doi.org/10.1126/science.263.5144.212` doi: 10.1126/science.263.5144.212

Conrad, C. P., & Lithgow-Bertelloni, C. (2002, October). How mantle slabs drive plate tectonics. *Science*, *298*(5591), 207–209. Retrieved from `https://doi.org/10.1126/science.1074161` doi: 10.1126/science.1074161

Conrad, C. P., & Lithgow-Bertelloni, C. (2004, October). The temporal evolution of plate driving forces: Importance of "slab suction" versus "slab pull" during the cenozoic. *Journal of Geophysical Research: Solid Earth*, *109*(B10). Retrieved from `https://doi.org/10.1029/2004jb002991` doi: 10.1029/2004jb002991

Craig, T. J. (2019, February). Accurate depth determination for moderate-magnitude earthquakes using global teleseismic data. *Journal of Geophysical Research: Solid Earth*, *124*(2), 1759–1780. Retrieved from `https://doi.org/10.1029/2018jb016902` doi: 10.1029/2018jb016902

Craig, T. J., & Copley, A. (2018, February). Forearc collapse, plate flexure, and seismicity within the downgoing plate along the sunda arc west of sumatra. *Earth and Planetary Science Letters*, *484*, 81–91. Retrieved from `https://doi.org/10.1016/j.epsl.2017.12.004` doi: 10.1016/j.epsl.2017.12.004

Craig, T. J., Copley, A., & Jackson, J. (2014, February). A reassessment of outer-rise seismicity and its implications for the mechanics of oceanic lithosphere. *Geophysical Journal International*, *197*(1), 63–89. Retrieved from `https://doi.org/10.1093/gji/ggu013` doi: 10.1093/gji/ggu013

Ekström, G., Nettles, M., & Dziewoński, A. (2012, June). The global CMT project

2004–2010: Centroid-moment tensors for 13, 017 earthquakes. *Physics of the Earth and Planetary Interiors*, *200-201*, 1–9. Retrieved from `https://doi.org/10.1016/j.pepi.2012.04.002` doi: 10.1016/j.pepi.2012.04.002

Elsasser, W. M. (1969). Convection and stress propagation in the upper mantle.

Emmerson, B., & McKenzie, D. (2007, August). Thermal structure and seismicity of subducting lithosphere. *Physics of the Earth and Planetary Interiors*, *163*(1-4), 191–208. Retrieved from `https://doi.org/10.1016/j.pepi.2007.05.007` doi: 10.1016/j.pepi.2007.05.007

Engdahl, E. R., & Scholz, C. H. (1977, October). A double benioff zone beneath the central aleutians: An unbending of the lithosphere. *Geophysical Research Letters*, *4*(10), 473–476. Retrieved from `https://doi.org/10.1029/gl004i010p00473` doi: 10.1029/gl004i010p00473

Engdahl, E. R., van der Hilst, R., & Buland, R. (1998). Global teleseismic earthquake relocation with improved travel times and procedures for depth determination. *Bulletin of the Seismological Society of America*, *88*(3), 722–743.

England, P., & Wilkins, C. (2004, December). A simple analytical approximation to the temperature structure in subduction zones. *Geophysical Journal International*, *159*(3), 1138–1154. Retrieved from `https://doi.org/10.1111/j.1365-246x.2004.02419.x` doi: 10.1111/j.1365-246x.2004.02419.x

Faccenda, M. (2014, February). Water in the slab: A trilogy. *Tectonophysics*, *614*, 1–30. Retrieved from `https://doi.org/10.1016/j.tecto.2013.12.020` doi: 10.1016/j.tecto.2013.12.020

Forsyth, D., & Uyeda, S. (1975, oct). On the relative importance of the driving forces of plate motion. *Geophysical Journal International*, *43*(1), 163–200. Retrieved from `http://dx.doi.org/10.1111/j.1365-246x.1975.tb00631.x` doi: 10.1111/j.1365-246x.1975.tb00631.x

Fuenzalida, A., Schurr, B., Lancieri, M., Sobiesiak, M., & Madariaga, R. (2013, May). High-resolution relocation and mechanism of aftershocks of the 2007 tocopilla (chile) earthquake. *Geophysical Journal International*, *194*(2), 1216–1228. Retrieved from `https://doi.org/10.1093/gji/ggt163` doi: 10.1093/gji/ggt163

Fujita, K., & Kanamori, H. (1981a, July). Double seismic zones and stresses of intermediate depth earthquakes. *Geophysical Journal International*, *66*(1), 131–

156. Retrieved from `https://doi.org/10.1111/j.1365-246x.1981.tb05950` `.x` doi: 10.1111/j.1365-246x.1981.tb05950.x

Fujita, K., & Kanamori, H. (1981b, July). Double seismic zones and stresses of intermediate depth earthquakes. *Geophysical Journal International*, *66*(1), 131–156. Retrieved from `https://doi.org/10.1111/j.1365-246x.1981.tb05950` `.x` doi: 10.1111/j.1365-246x.1981.tb05950.x

Gerardi, G., & Ribe, N. M. (2018, June). Boundary element modeling of two-plate interaction at subduction zones: Scaling laws and application to the aleutian subduction zone. *Journal of Geophysical Research: Solid Earth*, *123*(6), 5227–5248. Retrieved from `https://doi.org/10.1002/2017jb015148` doi: 10.1002/2017jb015148

Ghosh, A., Holt, W. E., & Flesch, L. M. (2009, November). Contribution of gravitational potential energy differences to the global stress field. *Geophysical Journal International*, *179*(2), 787–812. Retrieved from `https://doi.org/` `10.1111/j.1365-246x.2009.04326.x` doi: 10.1111/j.1365-246x.2009.04326.x

Goes, S., Capitanio, F., Morra, G., Seton, M., & Giardini, D. (2011). Signatures of downgoing plate-buoyancy driven subduction in cenozoic plate motions. *Physics of the Earth and Planetary Interiors*, *184*(1-2), 1–13. Retrieved from `https://doi.org/10.1016/j.pepi.2010.10.007`

Green, H. W., & Houston, H. (1995). The mechanics of deep earthquakes. *Annual Review of Earth and Planetary Sciences*, *23*(1), 169–213.

Gurnis, M., Ritsema, J., Heijst, H.-J. V., & Zhong, S. (2000, August). Tonga slab deformation: The influence of a lower mantle upwelling on a slab in a young subduction zone. *Geophysical Research Letters*, *27*(16), 2373–2376. Retrieved from `https://doi.org/10.1029/2000gl011420` doi: 10.1029/2000gl011420

Gutenberg, B., & Richter, C. (1954). *Seismicity of the world and associated phenomena.* Princeton University Press, Princeton, NJ.

Gutscher, M.-A., Spakman, W., Bijwaard, H., & Engdahl, E. R. (2000, October). Geodynamics of flat subduction: Seismicity and tomographic constraints from the andean margin. *Tectonics*, *19*(5), 814–833. Retrieved from `https://doi.org/10.1029/1999tc001152` doi: 10.1029/1999tc001152

Hacker, B. R., Peacock, S. M., Abers, G. A., & Holloway, S. D. (2003, January). Subduction factory 2. are intermediate-depth earthquakes in subducting slabs

linked to metamorphic dehydration reactions? *Journal of Geophysical Research: Solid Earth*, *108*(B1). Retrieved from https://doi.org/10.1029/2001jb001129 doi: 10.1029/2001jb001129

Hasegawa, A., Umino, N., & Takagi, A. (1978, May). Double-planed structure of the deep seismic zone in the northeastern japan arc. *Tectonophysics*, *47*(1-2), 43–58. Retrieved from https://doi.org/10.1016/0040-1951(78)90150-6 doi: 10.1016/0040-1951(78)90150-6

Hayes, G. P., Moore, G. L., Portner, D. E., Hearne, M., Flamme, H., Furtney, M., & Smoczyk, G. M. (2018, August). Slab2, a comprehensive subduction zone geometry model. *Science*, *362*(6410), 58–61. Retrieved from https://doi.org/10.1126/science.aat4723 doi: 10.1126/science.aat4723

Hayes, G. P., Wald, D. J., & Johnson, R. L. (2012, January). Slab1.0: A three-dimensional model of global subduction zone geometries. *Journal of Geophysical Research: Solid Earth*, *117*(B1), n/a–n/a. Retrieved from https://doi.org/10.1029/2011jb008524 doi: 10.1029/2011jb008524

House, L. S., & Jacob, K. H. (1982, February). Thermal stresses in subducting lithosphere can explain double seismic zones. *Nature*, *295*(5850), 587–589. Retrieved from https://doi.org/10.1038/295587a0 doi: 10.1038/295587a0

Hunter, J., & Watts, A. (2016, July). Gravity anomalies, flexure and mantle rheology seaward of circum-pacific trenches. *Geophysical Journal International*, *207*(1), 288–316. Retrieved from https://doi.org/10.1093/gji/ggw275 doi: 10.1093/gji/ggw275

Imanishi, K., Ando, R., & Kuwahara, Y. (2012, May). Unusual shallow normal-faulting earthquake sequence in compressional northeast japan activated after the 2011 off the pacific coast of tohoku earthquake. *Geophysical Research Letters*, *39*(9), n/a–n/a. Retrieved from https://doi.org/10.1029/2012gl051491 doi: 10.1029/2012gl051491

Isacks, B., & Barazangi, M. (1977). Geometry of benioff zones: Lateral segmentation and downwards bending of the subducted lithosphere. In *Island arcs, deep sea trenches and back-arc basins* (pp. 99–114). American Geophysical Union. Retrieved from https://doi.org/10.1029/me001p0099 doi: 10.1029/me001p0099

Isacks, B., & Molnar, P. (1969, sep). Mantle Earthquake Mechanisms and the Sink-

ing of the Lithosphere. *Nature*, *223*(5211), 1121–1124. Retrieved from `http://dx.doi.org/10.1038/2231121a0` doi: 10.1038/2231121a0

Isacks, B., & Molnar, P. (1971). Distribution of stresses in the descending lithosphere from a global survey of focal-mechanism solutions of mantle earthquakes. *Review of Geophysics*, *9*(1), 103. Retrieved from `http://dx.doi.org/10.1029/rg009i001p00103` doi: 10.1029/rg009i001p00103

Jackson, J. (1980, May). Errors in focal depth determination and the depth of seismicity in iran and turkey. *Geophysical Journal International*, *61*(2), 285–301. Retrieved from `https://doi.org/10.1111/j.1365-246x.1980.tb04318.x` doi: 10.1111/j.1365-246x.1980.tb04318.x

Kawakatsu, H. (1986a). Double seismic zones: Kinematics. *Journal of Geophysical Research*, *91*(B5), 4811. Retrieved from `https://doi.org/10.1029/jb091ib05p04811` doi: 10.1029/jb091ib05p04811

Kawakatsu, H. (1986b). Downdip tensional earthquakes beneath the tonga arc: A double seismic zone? *Journal of Geophysical Research*, *91*(B6), 6432. Retrieved from `https://doi.org/10.1029/jb091ib06p06432` doi: 10.1029/jb091ib06p06432

Kirby, S., Engdahl, R. E., & Denlinger, R. (2013, March). Intermediate-depth intraslab earthquakes and arc volcanism as physical expressions of crustal and uppermost mantle metamorphism in subducting slabs. In *Subduction top to bottom* (pp. 195–214). American Geophysical Union. Retrieved from `https://doi.org/10.1029/gm096p0195` doi: 10.1029/gm096p0195

Kita, S., Okada, T., Hasegawa, A., Nakajima, J., & Matsuzawa, T. (2010, December). Existence of interplane earthquakes and neutral stress boundary between the upper and lower planes of the double seismic zone beneath tohoku and hokkaido, northeastern japan. *Tectonophysics*, *496*(1-4), 68–82. Retrieved from `https://doi.org/10.1016/j.tecto.2010.10.010` doi: 10.1016/j.tecto.2010.10.010

Lemoine, A., Madariaga, R., & Campos, J. (2002, September). Slab-pull and slab-push earthquakes in the mexican, chilean and peruvian subduction zones. *Physics of the Earth and Planetary Interiors*, *132*(1-3), 157–175. Retrieved from `https://doi.org/10.1016/s0031-9201(02)00050-x` doi: 10.1016/s0031-9201(02)00050-x

Lister, G., Kennett, B., Richards, S., & Forster, M. (2008). Boudinage of a stretching slablet implicated in earthquakes beneath the hindu kush. *Nature Geoscience*, *1*(3), 196.

Lorinczi, P., & Houseman, G. (2009, September). Lithospheric gravitational instability beneath the southeast carpathians. *Tectonophysics*, *474*(1-2), 322–336. Retrieved from https://doi.org/10.1016/j.tecto.2008.05.024 doi: 10.1016/j.tecto.2008.05.024

Manea, V., & Gurnis, M. (2007, December). Subduction zone evolution and low viscosity wedges and channels. *Earth and Planetary Science Letters*, *264*(1-2), 22–45. Retrieved from https://doi.org/10.1016/j.epsl.2007.08.030 doi: 10.1016/j.epsl.2007.08.030

McAdoo, D. C., Caldwell, J. G., & Turcotte, D. L. (1978, July). On the elastic-perfectly plastic bending of the lithosphere under generalized loading with application to the kuril trench. *Geophysical Journal International*, *54*(1), 11–26. Retrieved from https://doi.org/10.1111/j.1365-246x.1978.tb06753.x doi: 10.1111/j.1365-246x.1978.tb06753.x

McCrory, P. A., Blair, J. L., Waldhauser, F., & Oppenheimer, D. H. (2012, September). Juan de fuca slab geometry and its relation to wadati-benioff zone seismicity. *Journal of Geophysical Research: Solid Earth*, *117*(B9). Retrieved from https://doi.org/10.1029/2012jb009407 doi: 10.1029/2012jb009407

McKenzie, D. P. (1969, September). Speculations on the consequences and causes of plate motions. *Geophysical Journal International*, *18*(1), 1–32. Retrieved from https://doi.org/10.1111/j.1365-246x.1969.tb00259.x doi: 10.1111/j.1365-246x.1969.tb00259.x

Molnar, P., & Bendick, R. (2019, May). Seismic moments of intermediate-depth earthquakes beneath the hindu kush: Active stretching of a blob of sinking thickened mantle lithosphere? *Tectonics*. Retrieved from https://doi.org/10.1029/2018tc005336 doi: 10.1029/2018tc005336

Nothard, S., McKenzie, D., Haines, J., & Jackson, J. (1996, November). Gaussian curvature and the relationship between the shape and the deformation of the tonga slab. *Geophysical Journal International*, *127*(2), 311–327. Retrieved from https://doi.org/10.1111/j.1365-246x.1996.tb04722.x doi: 10.1111/j.1365-246x.1996.tb04722.x

Peacock, S. M. (2001). Are the lower planes of double seismic zones caused by serpentine dehydration in subducting oceanic mantle? *Geology*, *29*(4), 299. Retrieved from https://doi.org/10.1130/0091-7613(2001)029<0299: atlpod>2.0.co;2 doi: 10.1130/0091-7613(2001)029⟨0299:atlpod⟩2.0.co;2

Ribe, N. M. (2001, apr). Bending and stretching of thin viscous sheets. *Journal of Fluid Mechanics*, *433*, 135–160. Retrieved from http://dx.doi.org/10.1017/ s0022112000003360 doi: 10.1017/s0022112000003360

Ribe, N. M. (2010, feb). Bending mechanics and mode selection in free subduction: a thin-sheet analysis. *Geophysical Journal International*, *180*(2), 559–576. Retrieved from http://dx.doi.org/10.1111/j.1365-246x.2009.04460.x doi: 10.1111/j.1365-246x.2009.04460.x

Richter, F. M. (1979, November). Focal mechanisms and seismic energy release of deep and intermediate earthquakes in the tonga-kermadec region and their bearing on the depth extent of mantle flow. *Journal of Geophysical Research: Solid Earth*, *84*(B12), 6783–6795. Retrieved from https://doi.org/10.1029/ jb084ib12p06783 doi: 10.1029/jb084ib12p06783

Rietbrock, A., & Waldhauser, F. (2004, May). A narrowly spaced double-seismic zone in the subducting nazca plate. *Geophysical Research Letters*, *31*(10), n/a– n/a. Retrieved from https://doi.org/10.1029/2004gl019610 doi: 10.1029/ 2004gl019610

Romeo, I., & Álvarez-Gómez, J. (2018). Lithospheric folding by flexural slip in subduction zones as source for reverse fault intraslab earthquakes. *Scientific reports*, *8*(1), 1367.

Samowitz, I. R., & Forsyth, D. W. (1981). Double seismic zone beneath the mariana island arc. *Journal of Geophysical Research*, *86*(B8), 7013. Retrieved from https://doi.org/10.1029/jb086ib08p07013 doi: 10.1029/ jb086ib08p07013

Sandiford, D., & Moresi, L. (2019, June). Improving subduction interface implementation in dynamic numerical models. *Solid Earth*, *10*(3), 969–985. Retrieved from https://doi.org/10.5194/se-10-969-2019 doi: 10.5194/se-10 -969-2019

Sandiford, D., Moresi, L., Sandiford, M., & Yang, T. (2019, December). Geometric controls on flat slab seismicity. *Earth and Planetary Science Letters*, *527*,

1374   115787.   Retrieved from `https://doi.org/10.1016/j.epsl.2019.115787`

1375   doi: 10.1016/j.epsl.2019.115787

1376 Sandiford, M., Coblentz, D., & Schellart, W. P.   (2005).   Evaluating slab-plate

1377   coupling in the indo-australian plate.   *Geology*, *33*(2), 113.   Retrieved from

1378   `https://doi.org/10.1130/g20898.1` doi: 10.1130/g20898.1

1379 Schellart, W. (2017). Andean mountain building and magmatic arc migration driven

1380   by subduction-induced whole mantle flow.   *Nature communications*, *8*(1),

1381   2010.

1382 Schellart, W. P.   (2004, April).   Quantifying the net slab pull force as a driv-

1383   ing mechanism for plate tectonics.   *Geophysical Research Letters*, *31*(7),

1384   n/a–n/a.   Retrieved from `https://doi.org/10.1029/2004gl019528`   doi:

1385   10.1029/2004gl019528

1386 Seno, T., & Yamanaka, Y.   (2013, March).   Double seismic zones, compressional

1387   deep trench-outer rise events, and superplumes.   In *Subduction top to bottom*

1388   (pp. 347–355).   American Geophysical Union.   Retrieved from `https://doi`

1389   `.org/10.1029/gm096p0347` doi: 10.1029/gm096p0347

1390 Shillington, D. J., Bécel, A., Nedimović, M. R., Kuehn, H., Webb, S. C., Abers,

1391   G. A., . . . Mattei-Salicrup, G. A. (2015). Link between plate fabric, hydration

1392   and subduction zone seismicity in alaska. *Nature Geoscience*, *8*(12), 961.

1393 Sippl, C., Schurr, B., Asch, G., & Kummerow, J.   (2018, May).   Seismicity struc-

1394   ture of the northern chile forearc from 100, 000 double-difference relocated

1395   hypocenters.   *Journal of Geophysical Research: Solid Earth*, *123*(5), 4063–

1396   4087.   Retrieved from `https://doi.org/10.1002/2017jb015384`   doi:

1397   10.1002/2017jb015384

1398 Sleep, N. H.   (1979).   The double seismic zone in downgoing slabs and the

1399   viscosity of the mesosphere.   *Journal of Geophysical Research*, *84*(B9),

1400   4565.   Retrieved from `https://doi.org/10.1029/jb084ib09p04565`   doi:

1401   10.1029/jb084ib09p04565

1402 Sleep, N. H.   (2012).   Constraint on the recurrence of great outer-rise earthquakes

1403   from seafloor bathymetry. *Earth, Planets and Space*, *64*(12), 19.

1404 Tsujimori, T., Sisson, V., Liou, J., Harlow, G., & Sorensen, S.   (2006, December).

1405   Very-low-temperature record of the subduction process: A review of world-

1406   wide lawsonite eclogites.   *Lithos*, *92*(3-4), 609–624.   Retrieved from `https://`

doi.org/10.1016/j.lithos.2006.03.054 doi: 10.1016/j.lithos.2006.03.054

Tsukahara, H. (1980). Physical conditions for double seismic planes of the deep seismic zone. *Journal of Physics of the Earth*, *28*(1), 1–15.

Turcotte, D., McAdoo, D., & Caldwell, J. (1978, June). An elastic-perfectly plastic analysis of the bending of the lithosphere at a trench. *Tectonophysics*, *47*(3-4), 193–205. Retrieved from https://doi.org/10.1016/0040-1951(78)90030-6 doi: 10.1016/0040-1951(78)90030-6

van Hunen, J., van den Berg, A. P., & Vlaar, N. J. (2004, August). Various mechanisms to induce present-day shallow flat subduction and implications for the younger earth: a numerical parameter study. *Physics of the Earth and Planetary Interiors*, *146*(1-2), 179–194. Retrieved from https://doi.org/10.1016/j.pepi.2003.07.027 doi: 10.1016/j.pepi.2003.07.027

van Summeren, J., Conrad, C. P., & Lithgow-Bertelloni, C. (2012, February). The importance of slab pull and a global asthenosphere to plate motions. *Geochemistry, Geophysics, Geosystems*, *13*(2), n/a–n/a. Retrieved from https://doi.org/10.1029/2011gc003873 doi: 10.1029/2011gc003873

Vassiliou, M., Hager, B., & Raefsky, A. (1984, February). The distribution of earthquakes with depth and stress in subducting slabs. *Journal of Geodynamics*, *1*(1), 11–28. Retrieved from https://doi.org/10.1016/0264-3707(84)90004-8 doi: 10.1016/0264-3707(84)90004-8

Wagner, L. S., & Okal, E. A. (2019, July). The pucallpa nest and its constraints on the geometry of the peruvian flat slab. *Tectonophysics*, *762*, 97–108. Retrieved from https://doi.org/10.1016/j.tecto.2019.04.021 doi: 10.1016/j.tecto.2019.04.021

Wang, K. (2002, September). Unbending combined with dehydration embrittlement as a cause for double and triple seismic zones. *Geophysical Research Letters*, *29*(18), 36–1–36–4. Retrieved from https://doi.org/10.1029/2002gl015441 doi: 10.1029/2002gl015441

Yang, T., Gurnis, M., & Zhan, Z. (2017, July). Trench motion-controlled slab morphology and stress variations: Implications for the isolated 2015 bonin islands deep earthquake. *Geophysical Research Letters*, *44*(13), 6641–6650. Retrieved from https://doi.org/10.1002/2017gl073989 doi: 10.1002/2017gl073989

Yang, T., Moresi, L., Gurnis, M., Liu, S., Sandiford, D., Williams, S., & Capi-

1440   tanio, F. A. (2019, July). Contrasted east asia and south america tectonics

1441   driven by deep mantle flow. *Earth and Planetary Science Letters*, *517*, 106–

1442   116. Retrieved from `https://doi.org/10.1016/j.epsl.2019.04.025` doi:

1443   10.1016/j.epsl.2019.04.025